The Meteoritical Society

Meteoritics & Planetary Science 43, Nr 10, 1605–1628 (2008)
Abstract available online at http://meteoritics.org

Polygonal impact craters in Argyre region, Mars: Implications for geology and cratering mechanics

T. ÖHMAN[1, 2*], M. AITTOLA[2], V.-P. KOSTAMA[2], J. RAITALA[2], and J. KORTENIEMI[2, 3]

[1]Department of Geosciences, Division of Geology, University of Oulu, P.O. Box 3000, FI-90014, Finland
[2]Department of Physical Sciences, Division of Astronomy, University of Oulu, P.O. Box 3000, FI-90014, Finland
[3]Institut für Planetologie, Westfälische Wilhelms-Universität, Wilhelm-Klemm-Strasse 10, D-48149 Münster, Germany
[*]Corresponding author. E-mail: teemu.ohman@oulu.fi

(Received 20 November 2007; revision accepted 15 April 2008)

Abstract–Impact craters are not always circular; sometimes their rims are composed of several straight segments. Such polygonal impact craters (PICs) are controlled by pre-existing target structures, mainly faults or other similar planes of weakness. In the Argyre region, Mars, PICs comprise ~17% of the total impact crater population (>7 km in diameter), and PICs are relatively more common in older geologic units. Their formation is mainly controlled by radial fractures induced by the Argyre and Ladon impact basins, and to a lesser extent by the basin-concentric fractures. Also basin-induced conjugate shear fractures may play a role. Unlike the PICs, ridges and graben in the Argyre region are mostly controlled by Tharsis-induced tectonism, with the ridges being concentric and graben radial to Tharsis. Therefore, the PICs primarily reflect an old impact basin-centered tectonic pattern, whereas Tharsis-centered tectonism responsible for the graben and the ridges has only minor influence on the PIC rim orientations.

According to current models of PIC formation, complex PICs should form through a different mechanism than simple PICs, leading to different orientations of straight rim segments. However, when simple and complex PICs from same areas are studied, no statistically significant difference can be observed. Hence, in addition to enhanced excavation parallel to the strike of fractures (simple craters) and slumping along the fracture planes (complex craters), we propose a third mechanism involving thrusting along the fracture planes. This model is applicable to both simple and small complex craters in targets with some dominating orientations of structural weakness.

POLYGONAL CRATERS AND THE PURPOSE OF THE STUDY

Impact cratering is the most profound geologic process in the solar system. Only in special circumstances can processes related to volcanism (Io, Venus) or plate tectonics (Earth) change the balance so that cratering has only a minor influence on the currently observable geology. Mars is a diverse planet in a sense that it has a very large population of impact craters ranging in size from small simple craters to huge impact basins, but also major tectonic structures and volcanic centers. Hence, Mars is an ideal site to study the poorly understood interplay between impact cratering and the tectonic structures of the target lithology.

Impact craters are not merely just circular holes in the ground. As was generally known from the early 1900s to the 1960s and 1970s, many craters on the Moon are not circular but distinctly polygonal (e.g., Fielder 1961, 1965; Baldwin 1963; Kopal 1966; Schultz 1976). Most commonly, the plan view of such a crater is partially hexagonal (Fig. 1). This was regarded as evidence in favor of a volcanic origin for the lunar craters, as many terrestrial volcanic craters and calderas are rather polygonal. However, a terrestrial example of a polygonal impact crater (PIC) was also well known. The square shape of the 1.2 km-diameter Meteor Crater (also known as Barringer Crater) had been known at least since the 1940s (Baldwin 1949; Fielder 1961). The square shape was clearly the result of two orthogonal regional joint sets affecting the cratering process, and not a result of later crater degradation (Shoemaker 1962, 1963; Roddy 1978).

The interaction of cratering process and planar, roughly vertical target structures (faults, joints, fractures, and other similar planes of weakness, henceforth collectively referred to as "fractures") was summed up by Eppler et al. (1983) in their two models for polygonal crater formation. Their first model suggests that in simple craters the excavation flow should progress more easily along the fractures, hence enlarging the crater in a direction parallel to the strike of the

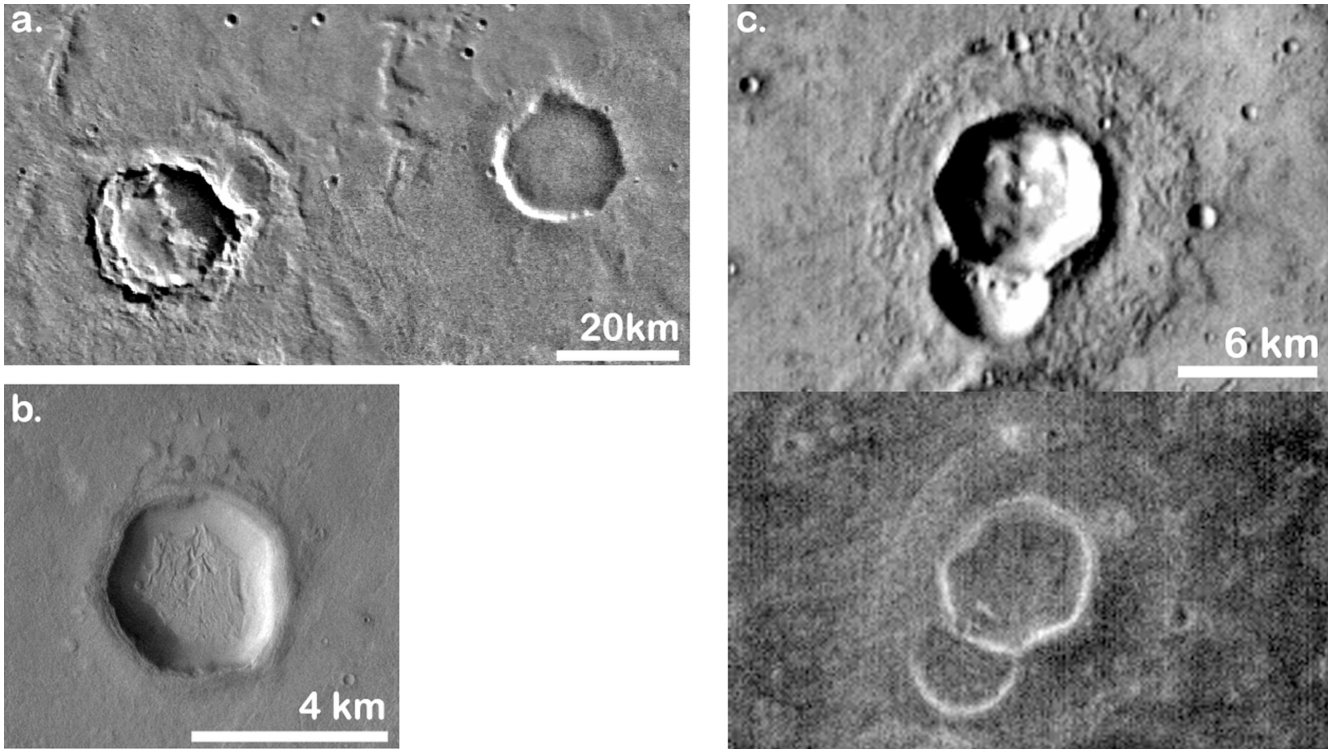

Fig. 1. Examples of polygonal impact craters in the Argyre region. a) Fresh (left) and degraded (right) PIC located at about 29.5°S 22.5°W, as seen using Viking MDIM 2.0 imagery. Both are typical complex PICs with a tendency towards a hexagonal shape. b) A simple PIC located northwest of Argyre basin (40.5°S 62.4°W) with typical sedimentary infill, as observed using part of THEMIS visual channel image V15168004. c) A fresh PIC showing incipient complex features located northeast of Argyre basin at 29.0°S 20.8°W, as observed using part of THEMIS daytime infrared image I17388002 (upper image) and part of THEMIS night-time infrared image I05887006 (lower image). Despite some differences, the same straight rim segments can be seen in both images regardless of the different viewing geometries. North is towards the top in all figures.

fractures. In an orthogonally jointed Meteor Crater-type target, the result would be a square crater with relatively straight rims making an angle of about 45° with the strike of the fractures.

In complex craters, dealt with in Eppler et al. (1983) model 2, the situation is notably different. Complex craters slump significantly in the modification stage (e.g., Gault et al. 1968; Melosh and Ivanov 1999 and references therein). According to Eppler et al. model, the slumping takes place along the pre-existing target fractures. Therefore, the crater expands in a direction perpendicular to the strike of the fractures. The end result is that the straight parts of the crater rim are parallel to the target fractures.

The best terrestrial example of a complex polygonal crater with rims reflecting target structures is the strikingly hexagonal Söderfjärden impact structure in western Finland, having a diameter of about 6.4 km (e.g., Abels 2003 and references therein). Elo et al. (1992) suggest that the 17–23 km diameter Lappajärvi impact structure's polygonal geophysical anomalies are due to crater formation being controlled by the pre-existing faults. Similarly, Floran and Dence (1976) propose that the 100 km-diameter Manicouagan impact structure went through structurally controlled slumping. Pre-existing faults have also been suggested to have played a major role in the modification of the ~260 km-diameter Sudbury impact structure (Spray et al. 2004). The 12 km-diameter Wells Creek structure presents an interesting case, where most of the faults radial to and concentric about the structure are parallel to the pre-existing joints, but the inner graben form roughly a square-shaped structure, with regional joint orientations being diagonal to it (Wilson and Stearns 1968). Hence, there is some evidence that the formation of terrestrial complex craters is indeed affected by the pre-existing target structures.

The studies of lunar PICs (e.g., Elston et al. 1971; Scott et al. 1977), as well as the few studies of Martian (Binder and McCarthy 1972; Schultz 1985; Öhman et al. 2005, 2006), Mercurian (Dzurisin 1978; Melosh and Dzurisin 1978; Strom et al. 1990), and Venusian (Aittola et al. 2007) PICs mainly have dealt with complex craters. Similarly, the brief remarks on the polygonality of some of the craters on the Saturnian satellite Iapetus (Denk et al. 2005; Porco et al. 2005) dealt also with complex craters. Thus, in planetary studies the causal link between target structures and complex PIC rim orientations seems to be well established.

In contrast, simple PICs have received substantially less attention. They have chiefly been observed but not much studied on asteroids 243 Ida, 253 Mathilde, and 433 Eros

(Belton et al. 1994; Veverka et al. 1997; Thomas et al. 1999; Zuber et al. 2000; Prockter et al. 2002), the nucleus of comet P/Wild-2 (Basilevsky and Keller 2006), and most recently on Mars (Watters 2006; Watters and Zuber 2007; for a more thorough discussion on previous PIC studies, see Öhman 2007). However, the correlation between fracture and straight rim segment orientations has only been fully established in one simple crater, i.e., the Meteor Crater.

The Meteor Crater-type of situation may not be universally true. This is emphasized by small-scale impact and explosion cratering experiments (Fulmer and Roberts 1963; Gault et al. 1968; see also Roddy and Davis 1977) that give a much more varied picture of the fracture/rim orientation relationship: straight rim segments may be parallel to target structures, or they may cut them at some angle. Thus further studies are clearly necessary.

As the correlation of (complex) PIC-rim orientation data with the target fractures is well known, they can be reliably used for tectonic interpretations (e.g., Scott et al. 1977; Dzurisin 1978; Melosh and Dzurisin 1978; Strom et al. 1990; Öhman et al. 2005). The validity of this approach is verified by studies showing that, at a regional scale, neither resolution (Binder and McCarthy 1972) nor the illumination geometry (Öhman et al. 2006) significantly affect the results. However, more detailed comparisons between PIC data and other tectonic indicators have so far been lacking. Thus, the purpose of this work is to study polygonal crater data in conjunction with data obtained from more widely studied tectonic features, and to see what these data can tell us about the geologic history of the study area. Another, equally important aim is to get a deeper insight into the influence of fractured target materials on the cratering process. We address these primary objectives through investigation of impact craters surrounding the Argyre impact basin of the southern hemisphere of Mars. As we have previously shown that this area hosts a population of polygonal craters having a wide range of different ages, as well as numerous graben and ridges (Öhman et al. 2006), it fits ideally our purposes.

GEOLOGIC BACKGROUND

Our study area (10°–74°W, 26°–58°S; Fig. 2) includes the Argyre impact basin and the surrounding geologic terrains. The basin, with a diameter of over 1500 km (Tanaka et al. 1992) and a depth of about 4 km (Mohit and Phillips 2007), is located in the southern highlands of Mars, southeast of the Tharsis rise and south to southeast of Valles Marineris (Wilhelms 1973; Wood and Head 1976). In the west and southwest, the study area extends to Aonia Terra, and in the east and southeast it reaches the western part of Noachis Terra, which is the type region of heavily cratered Noachian highlands. In contrast, the northwestern sector of our study area includes part of Thaumasia Planum (a geologic province that records Noachian tectonism, including incipient Valles Marineris development; Dohm et al. 2001a, 2001b), the ancient Thaumasia highlands (an ancient mountain range that records magnetic signatures and complex structures; Baker et al. 2007; Dohm et al. 2007), and a transition zone that straddles the Thaumasia highlands and the Argyre impact basin and includes Bosporos Planum (Scott and Tanaka 1986; Dohm et al. 2001a, 2001b). The sparsely cratered plains of Argyre Planitia cover most of the south central part of the study area.

Overall, Argyre basin appears rather undegraded when compared to the other large and well-studied impact basins on Mars, like the Hellas and Isidis basins (e.g., Spudis 1993). Crater counts suggest an age of only 3.83 ± 0.01 Ga for Argyre, whereas Isidis and Hellas may be 3.96 ± 0.01 and 3.99 ± 0.01 Ga old, respectively (Werner 2008). The well-preserved appearance of the Argyre basin may also be related to the thicker crust and deeper Moho in Argyre: the crust excavated by the Argyre impact had a minimum thickness of 23.7 km, compared to only 5.8 km and 6.6 km in Isidis and Hellas basins, respectively (Neumann et al. 2004; see also Mohit and Phillips 2007).

The Argyre basin may have contained a lake of great extent such that the standing water body would source Uzboi Valles to the north of the giant impact basin (e.g., Parker et al. 2000; Grant and Parker 2002; cf. Hiesinger and Head 2002). The morphology of the basin floor also suggests glacial activity for at least part of the recorded geologic history (e.g., Kargel and Strom 1992; Kargel 1993). The filling and the freezing of the suggested water body may be considered as the two major components in the evolution of the basin, although several different processes have influenced its unique appearance (e.g., Scott and Tanaka 1986; Head and Pratt 2001; Hiesinger and Head 2002).

The geologic units as defined by Scott and Tanaka (1986) and Tanaka and Scott (1987) were used in this study (Fig. 3). The oldest unit in the study area is the Noachian "hilly unit," Nplh. It is interpreted to result from the Argyre impact event, which uplifted and deformed old highland volcanics and impact breccia. Most parts of the study area are covered by two heavily cratered Noachian units, Npl_1 and Npl_2. The "cratered unit," Npl_1, has been interpreted to be materials emplaced during a period of heavy bombardment, being most likely a mixture of lava flows, pyroclastic material, and impact breccia. The younger Npl_2, or the "subdued crater unit," is interpreted to be thin lava flows and eolian deposits partly covering older rock materials. The "ridged unit," Nplr, is at least partly younger than the "cratered unit." The "ridges" are mostly interpreted to mark normal faults, though a minority of them could be either volcanic constructs or compressional features. Hesperian units are present in the central part of the Argyre basin, and in the western and northwestern part of the study area. The distribution of other geologic units as defined by Scott and Tanaka (1986) can be seen in Fig. 3.

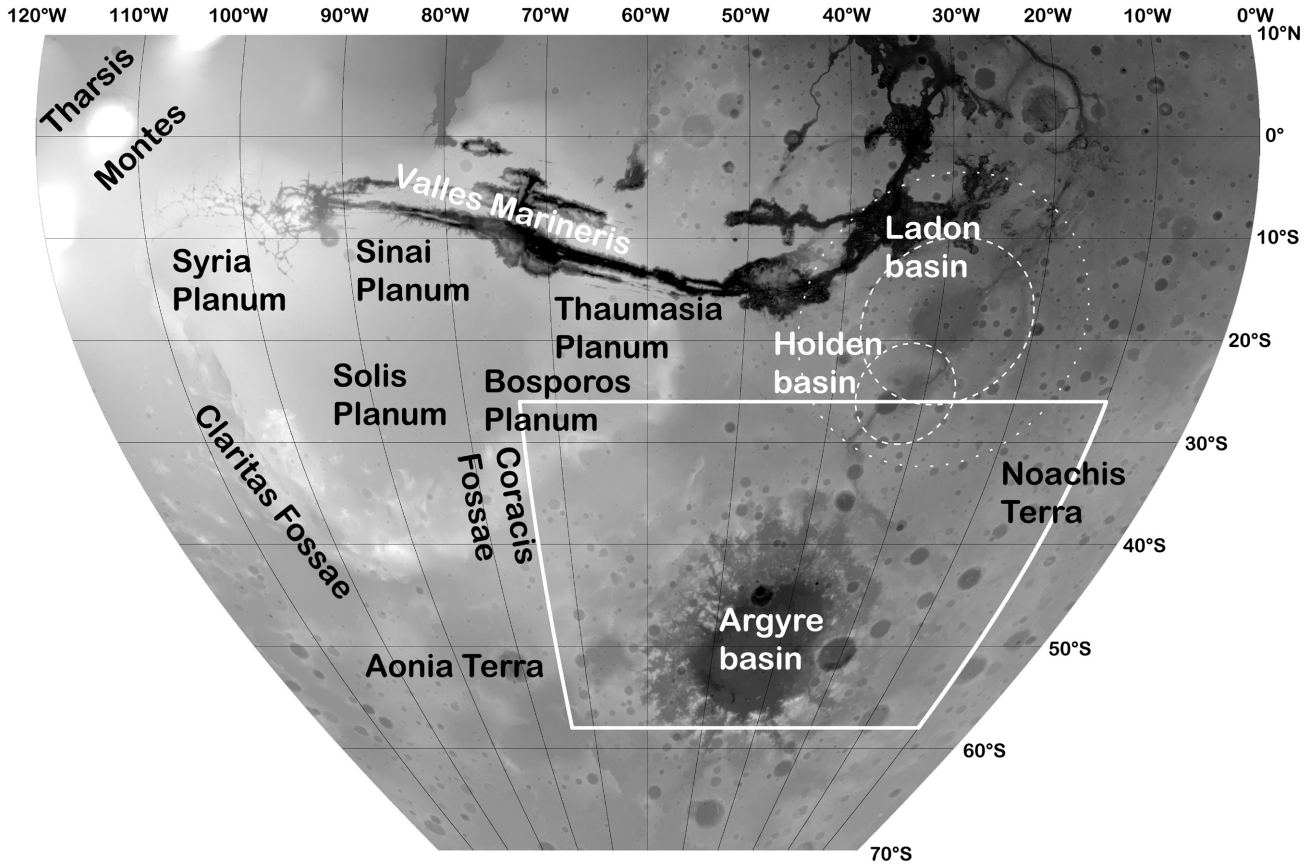

Fig. 2. A sinusoidal projection of MOLA topography (darker shades are low, whiter shades are high) of the study area (white box) which is located in the southern hemisphere of Mars, and the main geotectonic areas surrounding the Argyre region. The dashed circles indicate the 580 km-diameter Holden basin and the 975 km-diameter Ladon basin, and the dotted circle marks the proposed 1700 km-diameter outer ring of the Ladon basin (Schultz and Frey 1990).

Tectonic History of the Argyre Region

Schultz and Glicken (1979), Schultz et al. (1982), Pike and Spudis (1987), and Schultz and Frey (1990) among others studied ancient impact basins on Mars. In addition to Argyre, they also found other basins within and nearby our study area, including the Holden basin (Fig. 2; not to be mixed with the superposed Holden crater) centered at 25°S, 32°W and having a diameter of 580 km (Schultz et al. 1982; Pike and Spudis 1987). Holden basin lies mostly inside the larger Ladon basin (Fig. 2; centered at 18°S, 29°W), which probably has a diameter of about 975 km (Schultz et al. 1982), although outer rings could mark a deformational extent approaching 1700 km (Pike and Spudis 1987; Schultz and Frey 1990). The Ladon basin may be as old as the Noachian highlands, i.e., ~4.1 Ga (Werner 2008), and it is exceptionally deep (about 1.5 km) for an old basin its size (however, Mohit and Phillips (2007) use a diameter of only about 440 km for Ladon). In addition, a large, over 1600 km-diameter hypothetical ancient impact basin located at Solis Planum west from our study area was recognized from crustal thickness data by Frey et al. (2007).

It is generally known that impact basins, as well as smaller impact craters, create mainly radial and concentric tectonic structures around them (e.g., Baldwin 1963; Melosh 1976, 1978; Schultz et al. 1982; Wichman and Schultz 1989; Spudis 1993; Gurov et al. 2007). Such structures can also be seen in and surrounding the Argyre basin. Hodges (1980), while mapping the geology of the Argyre quadrangle, observed narrow concentric troughs, particularly in the northwest part of the study area (Fig. 3). Thomas and Masson (1984) studied the tectonics of the Argyre basin and observed many concentric escarpments. In addition, Thomas and Masson (1984) measured lineaments in the northwestern half of what they defined the "Nereidum Formation", which approximately corresponds to the "Argyre basin rim material" unit defined by Hodges (1980). They found a dominance of basin-radial lineaments, but also lineaments tangential to the basin were ubiquitous.

Thomas and Masson (1984) observed three pre-Argyre tectonic lineations, with the most significant one oriented NNE-NE. Other, less distinctive tectonic trends were oriented ESE and SSE (the lineaments in Fig. 3). Their conclusion was that the Argyre basin does not have any significant tectonic

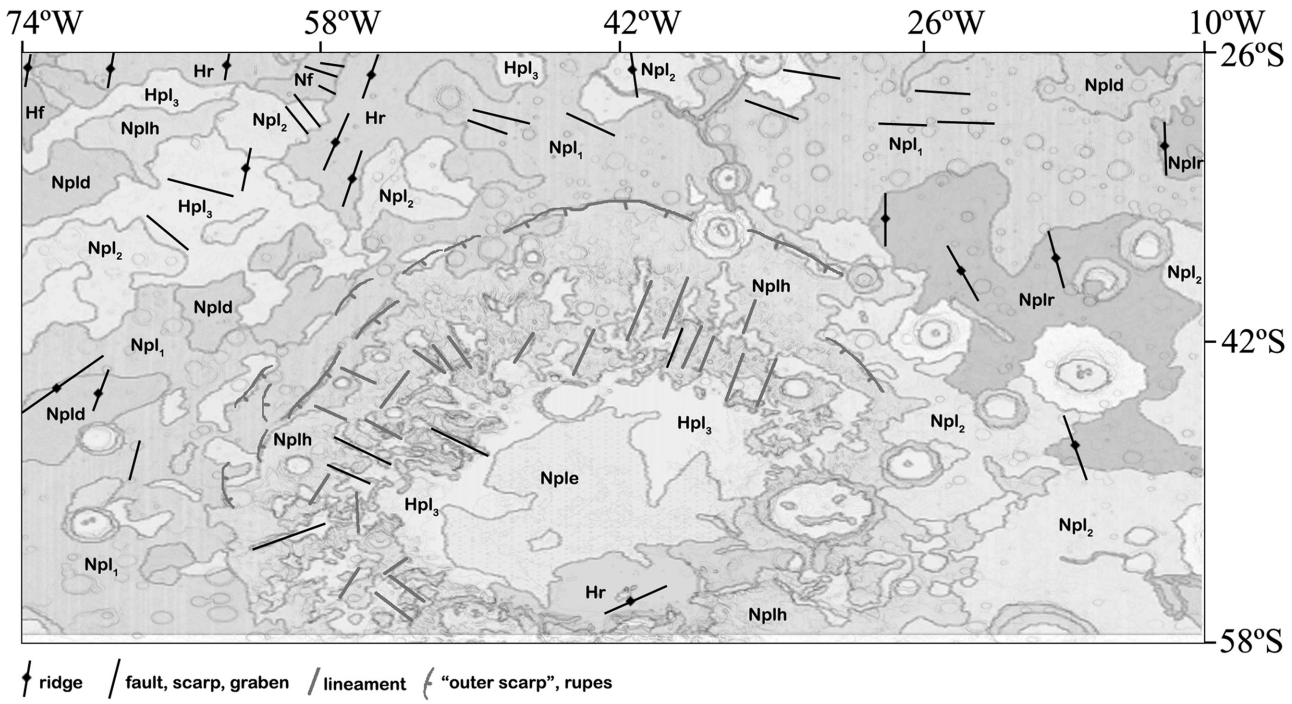

Fig. 3. A sketch of the main geologic units (Scott and Tanaka 1986) and tectonic structures in the study area. Note that the map of Scott and Tanaka (1986) does not quite reach the southernmost part of the study area. Ridges and faults, scarps and graben are simplified mainly after Scott and Tanaka (1986), with additional input from Dohm et al. (2001a) and Chicarro et al. (1985). Lineaments are simplified after Thomas and Masson (1984), and the "outer scarp" and rupes are after Thomas and Masson (1984) and Hodges (1980).

influence beyond an "outer scarp", which refers to Argyre Rupes situated about 1150 km southwest from the basin center (just beyond our study area) and smaller Argyre-concentric escarpments along the western and northern margins of the giant impact basin (Fig. 3). More recent investigation indicates that the Argyre impact-induced structural fabric in the crust may have influenced the formation of the southeast part of the Thaumasia plateau (Dohm and Tanaka 1999; Dohm et al. 2001a, 2001b), nearly 1500 km northwest of the basin center (see northwest corner of the study area in Fig. 2).

Schultz (1985) investigated scarps, graben, and channel-wall scarps in sections of the Argyre and Margaritifer Sinus regions, which partly cover our study area. His study is noteworthy because he used a few measurements of polygonal crater rims, which gave results similar to other tectonic indicators. Schultz made only a few measurements of the orientations of tectonic features in the Argyre area with dominant N-NNE and E-ENE trends of scarps and graben, respectively. In Margaritifer Sinus, NNE-trending scarps and channel-wall scarps are dominant. In addition, some scarps have an ESE-strike which parallels the main strike of the graben there. On the geologic map of the western equatorial region by Scott and Tanaka (1986), this ESE-trend of graben is apparent as well. N-NNE-trending ridges are yet another prominent tectonic feature type in their map.

A global study by Chicarro et al. (1985) focused on different types of ridges. They identified high and low-relief ridges in the Argyre region having a general NNW-NNE trend. A NNW-trending ridge orientation is evident in old cratered plains especially west of the Argyre basin, but in younger plains, the ridge orientation transitions more towards NNE-NE. In the eastern side of the basin, ridges on both old and younger terrain display a similar NNW-strike. The importance of this orientation is emphasized by the general NNW-striking ridge orientation that emerges after omitting the basin-concentric component from the data. After combining directions of all ridge types (except ring-forming ridges, which are probably buried impact craters), it appears that areas west from the Argyre basin are dominated by NNE-striking ridges. Ridges in the eastern and northeastern surroundings of the basin are striking NNW (Fig. 3). In the basin's northern side, a broader, generally northerly ridge strike is apparent (Chicarro et al. 1985).

Detailed and extensive geologic mapping has been carried out for the Thaumasia region (Dohm and Tanaka 1999; Dohm et al. 2001a) partly covering our study area. This work, which has major relevance for our research, details Tharsis-driven and pre-Tharsis activity. This record includes the initial formation of Tharsis during the Noachian (pre-Late Noachian), which comprises the forging of the Thaumasia plateau and the complex volcanic area of Syria Planum, especially highlighted during the Late Noachian through

spatial and temporal relations among rock materials and structures. The paleotectonic record of the Thaumasia region contains Syria-centered radial faults and concentric wrinkle ridges marking long-lived growth of the complex volcanic area, and faults radial and concentric about the central part of Valles Marineris related to incipient development of the vast canyon system, including magmatic-driven uplift at its central part (Dohm et al. 2001a, 2001b, 2007).

Especially in the northwestern part of our study area, a sharp decline of Tharsis- and Syria Planum-centered normal faulting occurred during Early–Late Hesperian. During the Late Hesperian, although the rifting in Valles Marineris probably continued, Tharsis activity transitioned from mainly widely distributed magmatic-tectonic to concentrated volcanism to forge the giant shield volcanoes and result in local tectonism (Dohm and Tanaka 1999; Anderson et al. 2001; Dohm et al. 2001a). The Thaumasia region may also record a pre-Tharsis phase of plate tectonism, as recorded by the ancient mountain ranges, Thaumasia highlands, and Coprates rise, marked by magnetic signatures, a generally high density of impact craters, and complex structure (Baker et al. 2007; Dohm et al. 2007) consistent in many respects with other ancient geologic provinces of the southern cratered highlands (e.g., Dohm et al. 2002, 2005; Fairén et al. 2002; Connerney et al. 2005; Baker et al. 2007).

Coracis Fossae, a part of the Thaumasia region, extends along the northwestern margin of block A (Fig. 2; for block division, see Fig. 4) of our study area. Coracis Fossae tectonism is associated with relatively small promontories that have been interpreted as volcanoes (Dohm and Tanaka 1999; Dohm et al. 2001a; Grott et al. 2005). The extensional tectonism at Coracis Fossae that resulted in the formation of the approximately N-trending graben system was active from the Noachian to the Early Hesperian (Dohm and Tanaka 1999).

Another prominent system of graben, Claritas Fossae, almost reaches our study area just west of block E (Fig. 2). The southeastern-most graben of Claritas Fossae are generally NNW-trending. Claritas Fossae-related faulting was substantially longer lived than in Coracis Fossae, as it commenced in Early–Middle Noachian, declined in Late Noachian and substantially diminished during the Late Hesperian/Amazonian (Dohm and Tanaka 1999).

In general, the previous studies suggest that the tectonics of the study area is mostly controlled by the Argyre impact and the resulting basin-radial and basin-concentric structures. The long-lasting and complex tectonism related to the Tharsis bulge (and Syria Planum) has also made a significant overprint in the region, highlighted by the largely Tharsis-concentric ridges and generally Tharsis-radial faults and graben (Scott and Tanaka 1986; Dohm and Tanaka 1999; Dohm et al. 2001a). Especially prominent are the generally NW-trending graben located northwest of the basin. However, in the most highly cratered terrains of the Argyre basin region, features radial to Tharsis are mostly lacking (Schultz 1985).

DATA AND METHODS

The primary data set for this study was the Mars mosaicked digital image model (MDIM 2.0), which has a favorable illumination geometry, continuous global coverage, and adequate resolution (231.4 m/pixel at the equator (Kirk et al. 2000)) for large-scale research. However, a downside of the Viking MDIM 2.0 is that the resolution gets poorer closer to the poles. This introduces a bias to the data, because smaller PICs become increasingly difficult to recognize in the southern parts of our study area. This must be kept in mind when inspecting the areal distribution of PICs. During the earliest phase of this and our previous work in the same area (Öhman et al. 2006), we actually extended the area to 72°S, but the work was not carried further than the initial stages because of the poor data quality so far south.

To be classified as a polygonal crater, the crater had to have at least two adjacent straight rim segments and a clearly discernible angle between the segments. The classification was made based on thorough visual inspection of each crater, as seen in MDIM 2.0. Also the craters classified either as simple or complex craters (see below) using Mars Odyssey Thermal Emission Imaging System (THEMIS) imagery were first classified as PICs using MDIM 2.0. To decrease the influence of subjectivity, the classification had to be agreed upon by two researchers. It is noteworthy, that craters displaying two straight rim segments on the opposite sides of the crater, which are connected by rim segments more or less following a circle, are *not polygonal* by our definition. Non-polygonal are also craters, whose apparent polygonality is primarily caused by post-impact processes (see Fig. 3 in Öhman et al. 2006 for examples). The classification is the same as in our previous studies (Öhman et al. 2005, 2006; Aittola et al. 2007), and thus the different studies are directly comparable. Because of the fairly strict criteria for classifying craters as polygonal, the amount of PICs found in this work represents the minimum number of polygonal craters in the area, and only a relatively small fraction of all craters which display straight rim segments.

The morphology of the polygonal craters in our study area was further studied by classifying them as either simple or complex craters. Typical Martian simple craters have flat floors due to sedimentary infilling. Hence, it is generally not possible to use the presence of a flat floor as an indication of an incipient complex crater, except in the case of the freshest craters. Therefore, the criteria for classifying a crater as a complex one included the presence of a central peak or a central pit, and rim terracing and scalloping, as well as the size of the crater. Especially in the case of highly degraded craters where the primary morphology of the rim is no longer visible, the diameter of the crater was an important criterion.

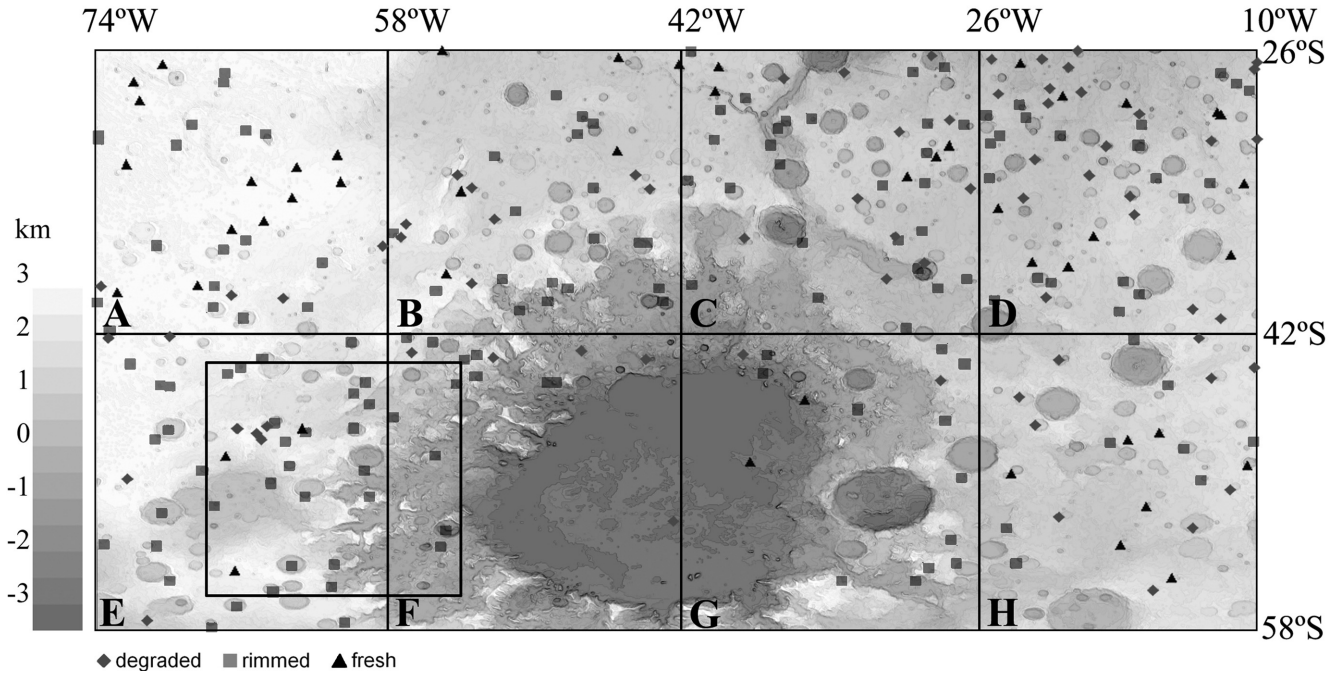

Fig. 4. The distribution and degradational stages of polygonal impact craters in the Argyre region, as well as the block divisions used in this work, plotted on MOLA topography in simple cylindrical projection. The black box in blocks E and F denotes the area whose PIC data was compared with the data west from Hellas basin (Fig. 9).

It should be noted, however, that although the average Martian simple/complex transition diameter is 7 km (e.g., Pike 1980; Garvin et al. 2003), the variation is large: the smallest Martian impact crater with apparently a true central peak has a diameter of only 1.5 km (Mouginis-Mark 1979), whereas some craters may retain their simple morphology up to a diameter of more than 10 km, even up to 18 km (Mouginis-Mark 1979; Pike 1980). Hence, all polygonal craters larger than 20 km in diameter were classified as complex craters without further study. The simple/complex classification of PICs less than 20 km in diameter was based on THEMIS infrared (~100 m/px) and visual channel images (17–35 m/px). Mars Reconnaissance Orbiter's High Resolution Imaging Science Experiment images (HiRISE) (0.25 m/px) were used to look for small simple PICs with a clear-cut relationship with the tectonic structures of the target.

The diameter and location data of PICs and non-polygonal craters was taken from Barlow's (2003) Catalog of Large Martian Impact Craters. The diameters and coordinates of the craters smaller than 5 km in diameter, or otherwise absent from Barlow's catalog, were measured from the United States Geological Survey's (USGS) shaded-relief hard-copy maps, and/or using data through the USGS Planetary GIS Web Server (PIGWAD).

The possible effect of target material on rim strikes and polygonality was studied by correlating each PIC with the encompassing geologic unit. The units were determined from the USGS geologic maps that cover extensive areas and therefore have consistent nomenclature (Scott and Tanaka 1986; Tanaka and Scott 1987). For classification purposes, all of the Hesperian units, and some of the Noachian units that are closely related to each other in time and interpreted origin (Scott and Tanaka 1986) were grouped together. The degradational stages of PICs are based on our previous work (fresh = preserved ejecta blanket, rimmed = no ejecta but rim preserved, degraded = rim mostly degraded; for further details on the degradation classification, see Öhman et al. 2006).

The study area was arbitrarily divided into eight 16° × 16° blocks (Fig. 4). This block division was the basis of the structural analysis. All the strike measurements of the structural features were calculated through on-screen analysis of MDIM 2.0 data using Adobe Photoshop. Measurements in Photoshop's coordinate system were then recalculated to actual geographic directions. Although no formal tests of the precision of the measurements were carried out, repeated measurements clearly imply that the precision of PIC-rim-strike measurements is about <5°. The measurement of tectonic lineaments (graben, ridges, and structurally controlled small channels) was carried out in a similar fashion, but the precision of the ridge and channel measurements is poorer due to their somewhat sinuous nature. Measurements were made from the rectilinear parts of the ridges or channels. Several measurements of each structure were made in cases where the orientation of the structure changed appreciably (around 15°).

The definition of graben in planetary geology is often

vague, and so it is in this study too. "Graben" in this study is an umbrella term, comprising all relatively rectilinear structures where some type of normal faulting can be observed or inferred, including graben, half-graben, faults, and escarpments. "Channels" are often closely related to graben, especially in the northwestern corner of the study area. Typically, a small channel can be seen in the bottom of a graben. In such cases, each structure was classified in only one category. The relatively small surficial channels (as opposed to larger structurally controlled channels), typically observed on crater rims for example, were omitted. Similarly, the largest more or less outflow-type of channels (e.g., Uzboi Vallis; see e.g., Grant and Parker 2002) were not included in the channel orientation measurements.

The structural data was presented in conventional rose diagrams, i.e., diagrams that use the radius of the sector for scaling, rather than the area of the sector as true circular histograms do. This visualization slightly overemphasizes the peaks in the diagrams (e.g., Cheeney 1983). Another factor affecting the interpretations based merely on visual inspection of the diagrams is the choice of class widths (i.e., directional intervals). However, the data was tested using 10° and 15° class widths, with no bearing on the conclusions nor the statistical tests (see below). As the main trends and not the details in the diagrams are of major interest in this study, we chose 15° intervals for most of the structural data (Figs. 7 and 8). For greater ease of following the subsequent discussion, major peaks in each of the diagrams were numbered clockwise from north.

In order to see if there is a statistically significant difference in the orientation distributions of straight rim segments between simple and complex craters, as well as between two different geologic units, we used a two-tailed, two-sample Kolmogorov-Smirnov-test (K-S-test) in the 95% confidence level (e.g., Cheeney 1983; Davis 2002; Sheskin 2004). The K-S-test is based on determining the largest difference between the cumulative sum frequency curves of the two samples. The data was tested using both 10° and 15° class intervals. The null hypotheses—expected to be rejected—were that the samples (i.e., straight rim segment orientations of simple and complex PICs, and in the two geologic units) are drawn from identical populations. Some of the results of the K-S-tests were also verified using the standard χ^2-test.

RESULTS

Distribution and the Geologic Units

Figure 4 displays the distribution and degradational stages of the 269 polygonal impact craters identified in this study. This should be regarded as the minimum number of PICs in the study area. Polygonal craters are most abundant in the old Noachian heavily cratered highland plains (Npl_1), northeast of the Argyre basin. Similar but a smaller accumulation of PICs can also be seen on the western side of the basin. All craters (including PICs) are very rare on the floor of the Argyre basin, and relatively few craters are present northwest from the basin, on the volcanic plains of Thaumasia and Bosporos Plana. Whereas fresh PICs with preserved ejecta blankets are more common in the geologic units interpreted to be volcanic plains, PICs with degraded rims are rarer when compared to the other parts of the study area. This clearly reflects the younger, Hesperian age of the plains.

The spatial differences in the *relative abundance* of PICs (i.e., the number of PICs compared to the total number of craters in the area in Barlow's [2003] catalog) in different parts of the study area follow the pattern of the absolute number of PICs (which follows the general crater density and thus the age of the surface; Table 1). Only craters larger than 7 km in diameter were included. This was to ensure both our survey of PICs and Barlow's catalog (which provided the number of non-polygonal craters) were complete and did not suffer from e.g., resolution problems. The highest relative abundance of PICs, about 22%, can be found in block E west from the basin. In block D northeast from the basin about 19% of all craters are polygonal. The lowest relative abundances (13%–15%) are in blocks A, B, and H.

Polygonal craters are more ubiquitous west (block E) of the Argyre basin than east (block H), despite the fact that in broad terms both blocks generally contain cratered highland plains materials. On the eastern side of the basin, however, the terrain is dominated by the younger Npl_2 unit in contrast to the older and even more highly cratered Npl_1 unit on the western side (Table 1). Therefore, the distribution of PICs roughly follows the geologic units. This is emphasized by the fact that the highest percentages of PICs are in blocks D and E, both of which are strongly dominated by the oldest unit that covers extensive areas, i.e., the "cratered unit" (Npl_1).

We also investigated whether the *amount of polygonality* of PICs, measured in terms of the number of straight rim segments of PICs, has any correlation with the geologic units. The results are given in Fig. 5. The percentages of different polygonality classes vary in different geologic units, but the general trend is obvious. There is no distinct preference of more polygonal craters in any of the geologic units, i.e., the *percentages* of each individual polygonality class are approximately the same in all of the geologic units, although the absolute numbers differ significantly (note that all Hesperian and some of the Noachian units have been combined). The most common polygonality class in all geologic units is the class of PICs with three straight rim segments with a percentage of about 35%–62%, whereas highly polygonal craters (5–6 straight sides) make always less than 10% of the total.

In block D northeast of the basin we studied if there is a difference between straight rim segment *orientations* of PICs located in two different geologic units, the older Npl1 unit (number of rim- strike measurements $n = 116$) and the slightly

younger (Scott and Tanaka 1986) Noachian ridged unit (Nplr, $n = 43$). Both 10° and 15° class intervals gave the same result: using the K–S-test in 95% confidence level, we did not see any statistically significant difference in the orientation distributions. However, when considering the meaning of this observation, it should be noted that the units Npl_1 and Nplr are not genetically or temporally significantly different from each other (Scott and Tanaka 1986). Other blocks in our study area do not have a meaningful number of measurements in two geologic units, so with the current data it is not possible to see if this observation has more general implications.

Diameter

The diameters of polygonal impact craters in the study region, as seen using Viking MDIM 2.0 imagery, span a wide size range. The smallest identified PIC was about 3.4 km in diameter, whereas the largest was 90.8 km. The diameter distribution of PICs compared to non-polygonal craters was studied to see if their size distributions differ. To determine this, only craters larger than 7 km were used, just as was the case for determining the relative abundance of PICs. The number of PICs over 7 km in diameter is 236. The inclusion of the 33 smaller craters, however, does not change the results significantly, but it does involve an element of uncertainty due to the inevitable incompleteness of both our and Barlow's (2003) catalog in smaller crater diameters.

The main results are given in Fig. 6. The size distributions of PICs and other craters are clearly distinct. The polygonal craters appear to be more abundant roughly in the 15 to 35 km diameter range. The largest discrepancy is in the size range of 20–25 km (when disregarding the smallest size range of 7–10 km). There are about 15% of all PICs in this size range, but only about 8% of other craters. When the diameter is normalized using 7 km as the average Martian simple/complex transition diameter (D_{tr}) (e.g., Pike 1980; Garvin et al. 2003), this "bulge" is about $2–5 \times D_{tr}$. To ensure data classification did not induce any spurious conclusions, both 5 km and 10 km class intervals were tested without major changes to the main result.

Structural Data: PICs, Ridges, Graben, and Channels

The results of the structural orientation measurements from all the blocks are compiled in Figs. 7 and 8, which include orientations of PICs, ridges, graben, and structurally controlled channels, as well as spatial relation among Argyre and Ladon basins, Tharsis, and Valles Marineris. For easier comparison with our previous work from the Hellas region (Öhman et al. 2005), and for better resolution, the rose diagrams in Fig. 9 are plotted in 10° class intervals rather than 15° intervals shown in Figs. 7 and 8.

As discussed above, current models predict that simple and complex polygonal craters should display different rim strike patterns. Because in the rose diagrams in Figs. 7 and 8 data from both simple and complex PICs are combined, it is essential to know if the presented data is a combination of two different sets of data, or if they present samples drawn from identical populations. In other words, are the rim strike distributions of simple and complex PICs really different? Due to the low number of simple PICs (42 simple PICs out of the total of 269), it was essential to combine two blocks to have a meaningful number of measurements. Hence, the straight rim segment strikes of simple and complex PICs were studied from four combined blocks. The results are presented in Fig. 10.

The straight rim orientation distributions of simple and complex PICs appear to be similar. This similarity was also verified by the K–S-test: in the 95% confidence level, we were not able to find any statistically significant differences in the rim strike distributions. The result in the combined blocks

Table 1. The relative abundances of PICs, and the absolute numbers of craters (>7 km in diameter), as well as the main geologic units in different blocks of the study area.

Block	PICs %	PICs	Others[1]	Total	Main units[2]
A	15%	26	144	170	Hpl_3, Npl_2, Hr
B	14%	29	185	214	Npl_1, Hr, Nplh
C	17%	33	161	194	Npl_1, Nplh
D	19%	51	216	267	Npl_1, Nplr
E	22%	44	152	196	Npl_1, Nplh
F	16%	14	73	87	Nple, Hpl_3, Nplh
G	16%	15	79	94	Hpl_3, Nplh, Nple
H	13%	24	158	182	Npl_2, Nplr
Mean/Total	17%	236	1168	1404	

[1]Taken from Barlow's (2003) catalog.
[2]Taken from Scott and Tanaka (1986) and Tanaka and Scott (1987).

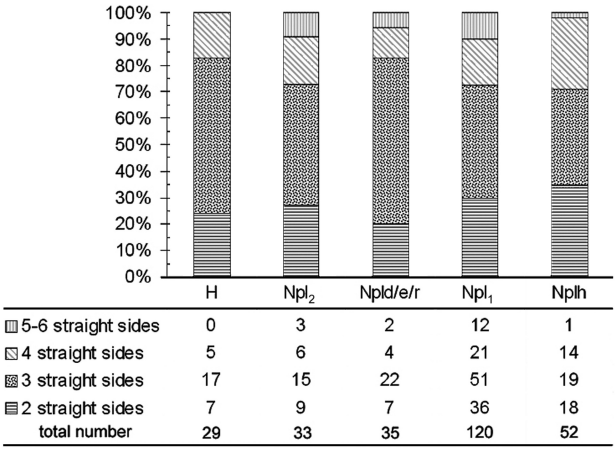

Fig. 5. The percentages of different polygonality classes (all degradational stages included), defined by the number of straight rim segments in different geologic units (Scott and Tanaka 1986; Tanaka and Scott 1987). Note that all the Hesperian units ("H"), as well as some of the closely related Noachian units ("Npld/e/r") have been combined. "Npl_1" unit includes also one crater in unit "Nf." The absolute numbers of PICs in different geologic units (provided in the table) are highly variable, which mainly reflects the crater densities in the units.

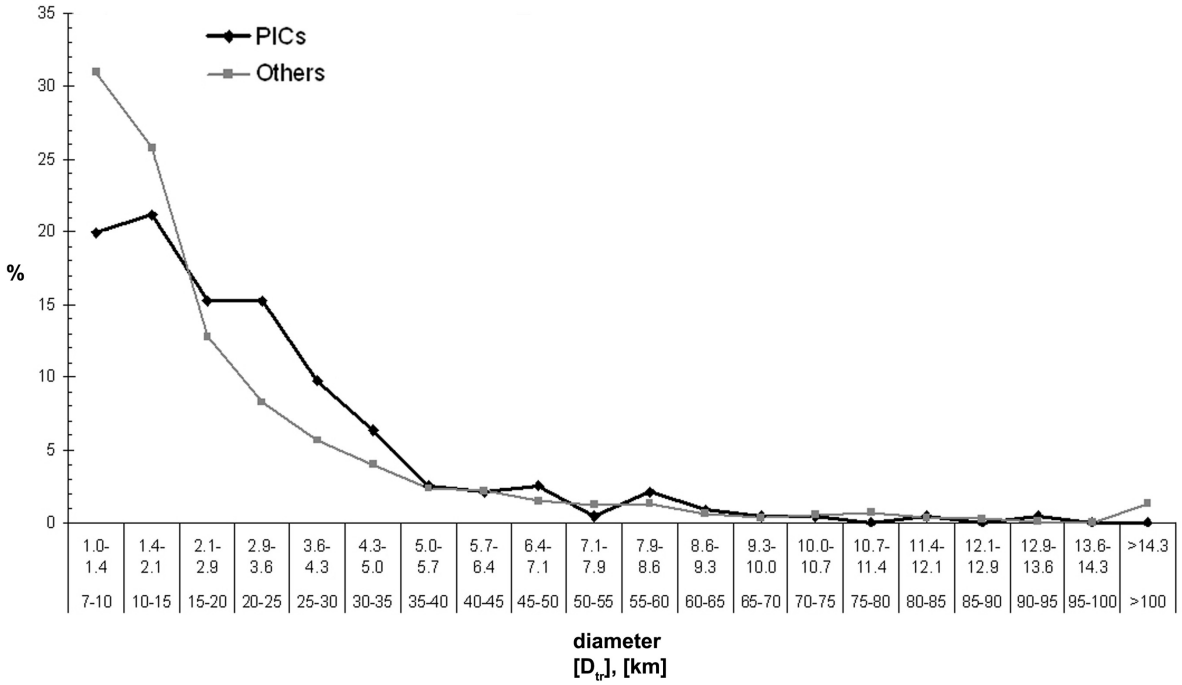

Fig. 6. The size distribution of polygonal ("PICs") and non-polygonal ("others") craters larger than 7 km in diameter in the Argyre region. Whereas the upper X-scale refers to multiples of the simple-to-complex transition diameter (D_{tr} = 7 km), the lower one is in kilometers.

A and B was also corroborated by the χ^2-test. Thus, it is justified to present orientation data from both simple and complex polygonal craters in one diagram.

Two features on the PIC rim strike diagrams from the northern half of the study area (blocks A–D, Figs. 7 and 8) remain constant in all of the diagrams: a peak in E-W direction, and another in NW direction. Crater rims oriented in ENE direction are conspicuously lacking in the whole region. In block E (Fig. 7) on the western side of the basin, three strong peaks dominate the rose diagram, the most pronounced orientation being E–W (peak E2). Block H (Fig. 8) on the opposite side of the basin displays a somewhat less straightforward picture with a wider roughly E-W peak (H2) in addition to other notable orientations, especially NNE (peak H1). In blocks F and G (Figs. 7 and 8), located on the western and eastern "rims," the dominant orientation of the polygonal crater rims is N-S (peaks F4 and G1), although other prominent orientations are also present.

Ridges mostly occur in the northern part of the study area, and the vast majority of them are in the northwestern corner, on the Late Noachian–Hesperian ridged plains of Bosporos and Thaumasia Plana (e.g., Dohm et al. 2001a). Their orientations are tightly clustered, and they transition from the NNE in block A, to NNW in block D (Figs. 7–8).

A gradual shift of the dominating orientation, similar to the one seen in the ridge orientations, can also be seen in the graben data from the northern half of the study area. In block A the graben strike is NW, turning to almost E-W in block D. An interesting feature is that in blocks A–C, where both PIC and graben measurements are numerous, the orientations do not coincide. Rather, graben seem to be oriented in a direction where the PIC diagrams have a gap.

Especially in the northwestern part of the study area (blocks A and B), channels are often found associated with graben. Therefore channels have the same orientations as the graben, but with a bit wider dispersion of the data. In blocks C and D (Fig. 8) this association vanishes, and the channels display a broad, generally northwesterly orientation.

In the southern half of the Argyre region, the graben data is more varied but also more scarce, thus hampering its reliability. However, in block E on the western side of the basin, a strong bimodal strike distribution (NNE and WNW) can be observed with an additional minor peak in NW orientation. Curiously the channel data from block E does not correlate with either of the bimodal peaks, but roughly with the minor peak (Fig. 7). The same NW orientation of graben dominates the few measurements (n = 13) made from block F on the western "rim" of the basin, whereas a NNW peak is evident in the equally few measurements on the eastern "rim" (block G).

DISCUSSION

Distribution, Geologic Units, and Size of PICs

In the Argyre region about 13%–22% of all impact craters (>7 km in diameter) are polygonal, showing that PICs are a generally common feature. This *relative* abundance of PICs seems to have some correlation with geologic units (as defined by Scott and Tanaka (1986), and Tanaka and Scott

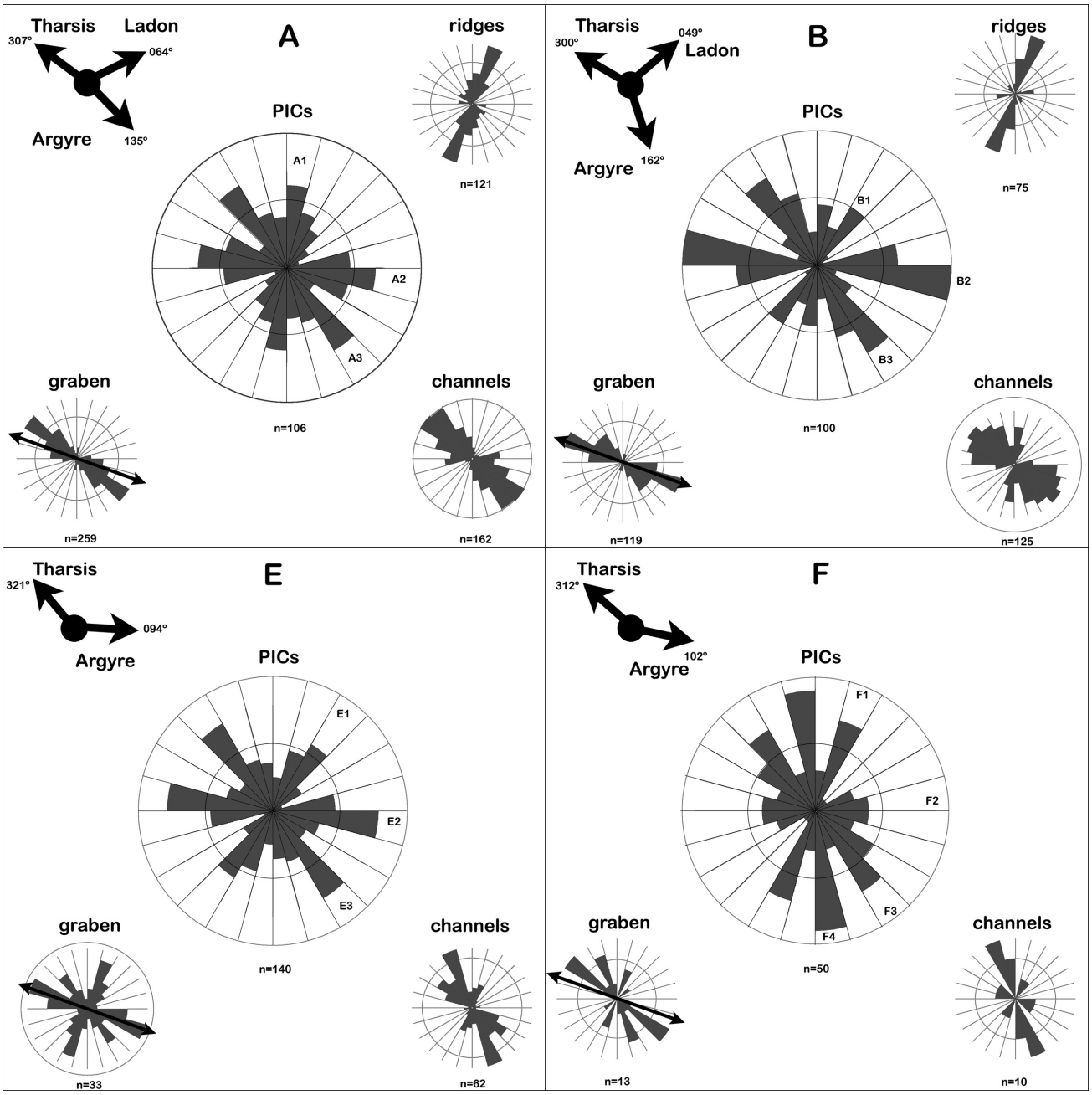

Fig. 7. Structural data from the blocks in the western half of our study area (see Fig. 4). All the rose diagrams in Figs. 7 and 8 are plotted using 15° class intervals. The inner and outer circles in PIC diagrams denote 10% and 20% of the total. In the ridge, graben, and channel diagrams, the circles mark 20% of the total. In the upper left corner of the set of diagrams, arrows pointing to the centers of the Argyre basin and the Tharsis bulge (the latter taken to be the caldera of Pavonis Mons; see, e.g., Dohm and Tanaka 1999) are also included for reference, as well the direction to the Ladon basin in some of the blocks located closest to it. The general trend of the Valles Marineris is displayed as a double-headed arrow in the graben diagrams.

(1987)): PICs are most abundant (~20% of craters) in areas dominated by the old geologic units, i.e., the Noachian cratered plains (Npl1) and units closely related to it (Table 1). Lowest relative abundances (~13%–15% of craters) are in areas where there is a major contribution of slightly younger Noachian plains (Npl_2) or Hesperian units (Hpl_3, Hr). Thus, PIC formation may be more common in older geologic units. It should be kept in mind, however, that the age of the unit which now hosts a crater does not tell practically anything about the age of the crater itself.

Figure 5 presents how the different geologic units of the Argyre region correspond with the amount of polygonality, as measured by the number of straight rim segments of PICs. An interesting result is that there is no obvious trend according to

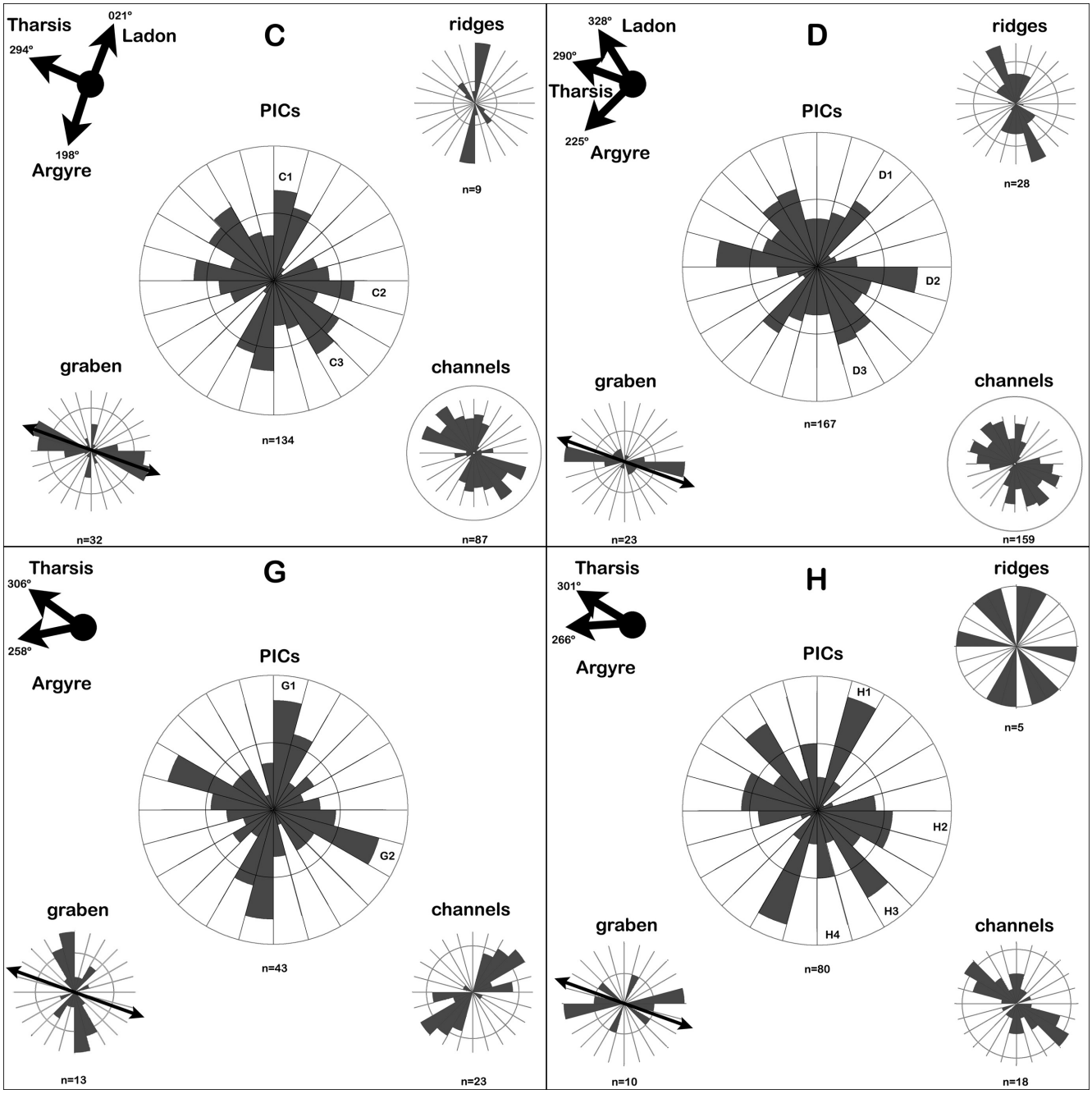

Fig. 8. Structural data from the eastern half of the study area. For the explanations of the diagrams, see Fig. 7.

relative age of the geologic unit. The most common polygonality class in all units is the PICs with three straight rim segments, although their percentage varies substantially (about 35%–62%). Highly polygonal craters (5–6 straight sides) always comprise less than 10% of the total number of PICs in each geologic unit. Thus, the percentages of each individual polygonality class are of the same order in all of the geologic units (note that all Hesperian and some of the Noachian units have been combined), and there does not appear to be any straightforward correlations between the amount of polygonality and the geologic unit. So although there seems to be a small preference of PIC formation in the older units (i.e., in old units a larger percentage of craters are polygonal than in younger units), the polygonal craters do not have a tendency to have more straight rim segments in these units.

The preference of PIC formation in the older units can be readily explained. Major crustal scale zones of weakness affecting the cratering process are probably very old, as has been suggested in the case of Mercurian polygonal craters

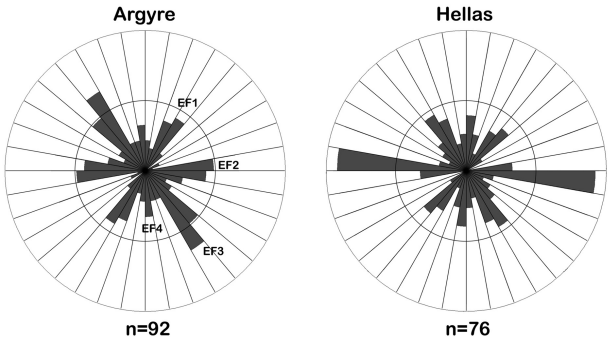

Fig. 9. Rose diagrams of PIC orientation data (using 10° class intervals) west of Argyre (see Fig. 4 for location) and Hellas basins (Hellas data taken from Öhman et al. 2005). The general appearance of the diagrams, especially the orientation of the peaks, is strikingly similar. This implies a possibility of similar origins.

(Dzurisin 1978; Strom et al. 1990). Provided the younger units are thick enough, they can impede the effect of the underlying structures on the crater formation process. In younger units, dominating structures may not have been developed, and hence no PICs are formed. However, when the PICs are formed, the number of straight rim segments does not seem to be dependent on the geologic unit. It is as likely to find a crater with several well-developed straight rim segments in old units as in younger units.

At least in the case of the main geologic units in block D, Npl_1 and Nplr, closely related in time, space, and interpreted origin, there does not seem to be any significant difference in the directional data indicated by the PICs. Thus, in the light of PIC data, at least the units Npl_1 and Nplr northeast of the Argyre basin apparently record similar tectonic histories. There are three possible reasons why the normal faults and compressional ridges that define the "ridged unit" Nplr do not lead to straight PIC rim orientations different from those in Npl_1. Firstly, the structures in Nplr may be parallel to the PIC-controlling structures (visible only in PIC-data) in Npl_1. Second, they may be younger than the structures affecting PIC formation and thus also younger than the PICs themselves, and hence the same old structure orientations would be responsible for PIC rim orientations in both Npl_1 and Nplr. The third option is that the faults and ridges defining the unit Nplr are rather surficial features, and therefore do not affect the crater formation significantly. It would be interesting to carry out a similar study in an area with two geologic units having distinctly different ages and interpreted tectonic histories.

The maximum depth of structures that can affect the PIC formation is the depth of the transient cavity (d_t). Assuming a transient cavity's depth/diameter—ratio of 1/3 (e.g., Melosh 1989), and using the formula provided by Croft (1985; again, the D_{tr} used is 7 km), it can be estimated that for the smallest complex craters studied in this work d_t is about two kilometers, for a typical 15–20 km PIC d_t is around 5 km, and for the largest craters in this study it is close to 20 km.

However, the formation of the rim is most likely not influenced by the deepest parts of the transient cavity where the material flows mainly downwards and outwards (e.g., Melosh 1989). Thus, the depth of the upwards oriented excavation provides a more reasonable estimate for the maximum depth of the structures affecting PIC formation. The excavation depth is about one tenth of the diameter of the transient cavity (Croft 1980; Melosh 1989; Spudis 1993). Therefore, for a typical PIC about 15–20 km in diameter, the structures controlling the crater rim orientations are likely not deeper than 1–2 km, and certainly not deeper than 5 km.

An average fresh 20 km-diameter Martian crater has a raised rim with a height of ~250 m (calculated with the equation by Garvin et al. (2003)), about half of which is due to structural uplift (Melosh 1989). However, as both fresh and highly degraded ("rimless") polygonal craters in the same area display similar rim strike orientations (Öhman et al. 2006), structures in the uppermost 100–150 m of the target are insignificant for a typical PIC formation. In other words, there either are no dominant structures in the uppermost layers of the target, and/or these surficial structures reflect deeper structures. Therefore, a rough estimate of the depth of the structures controlling the formation process of a typical PIC on Mars is ~100–1000 m.

The size distribution of PICs differs from that of the other craters in the study area (Fig. 6). PICs seem to "prefer" the mid-sized complex craters having diameters of about 15–35 km (~2–5 × D_{tr}). As with the relative abundance of PICs, this number can be compared with the results obtained from our on-going investigation of Venusian impact craters: similar to Mars, the size distributions of PICs and non-polygonal craters are different on Venus (Aittola et al. 2007). There, the PICs are relatively "excessively abundant" (with respect to other parts of the crater curves) in the size range of 12–25 km (~3–6 × D_{tr}). Pohn and Offield (1970) noted that lunar polygonal craters are most common in the size range of about 20–45 km (~1.3–3 × D_{tr}). Our preliminary data from the lunar nearside highlands are in a general agreement with this (Öhman et al. 2007). Therefore, a comparative analysis of PIC data from different planetary bodies indicates a possibility that there may be a specific size range with respect to the simple/complex transition, where craters develop straight rim segments more easily than in other sizes.

Ridges, Graben, and Channels

The ridges in the northern half of the Argyre region are clearly concentric to Tharsis, as has been noted before by e.g., Scott and Tanaka (1986). This becomes evident when comparing the orientations of ridges with the direction to Tharsis (Figs. 7 and 8). It should be noted that we concur with Kargel and Strom (1992) that the prominent linear features in the southern part of Argyre Planitia are eskers, and not (wrinkle) ridges. Hence, they were not included in our ridge data. Our ridge data from the northern part of the study area is in good agreement with the geologic mapping-based

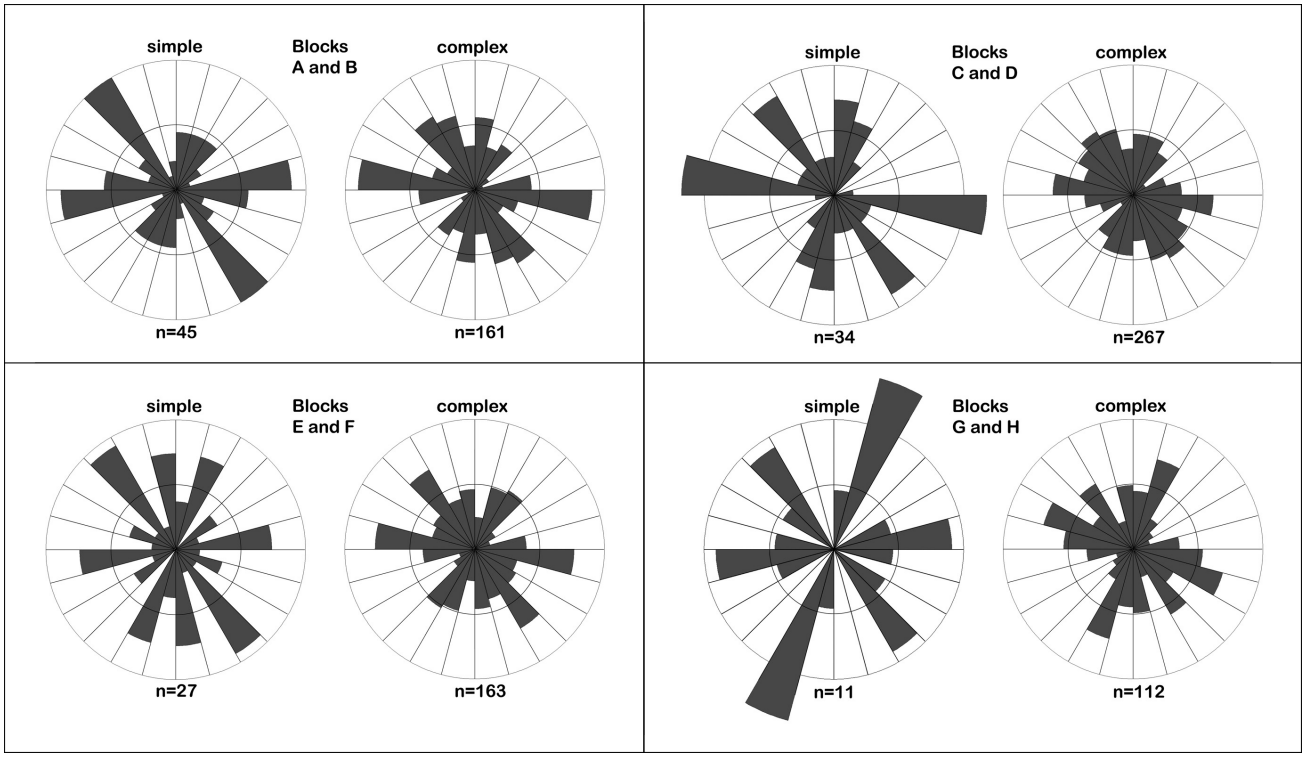

Fig. 10. Rose diagrams depicting the polygonal simple and complex PIC rim strike distributions in the *combined* blocks AB, CD, EF, and GH (for locations, see Fig. 4). Despite large differences in the number of measurements, the peaks and gaps are in the same locations, and thus, according to the K–S-test, there is no statistically significant difference in the rim strike distributions between simple and complex craters in the same area.

information of both Chicarro et al. (1985), and Scott and Tanaka (1986). Note, however, that the "ridges" mapped by Scott and Tanaka (1986) in their "ridged unit" (Nplr) included other structural features such as faults, whereas our "ridges" in cratered highlands are closer to typical wrinkle ridges in the volcanic plains. Therefore, we found very few ridges in the highlands where Scott and Tanaka (1986) mapped numerous ridges.

A shift in the orientations of graben, similar to the one observed with ridges, is also apparently a reflection of the influence of faulting radial to Tharsis. The graben in the northern half of the study area are also roughly parallel to the general trend of Valles Marineris. Therefore it seems clear that the graben in the northern part of the study area are mainly caused by Tharsis, which includes tectonism possibly associated with the formation of Valles Marineris (e.g., Dohm et al. 2001a, 2001b, 2007). The older tectonism related to the Argyre impact or pre-Argyre tectonism (Thomas and Masson 1984) apparently has not had any major influence in the graben orientations in the northern half of the study area.

In the southern half of the study area the picture emerging from the graben data is not so clear. Mainly this is because the graben are so rare (except in block E) that any truly reliable analysis is impossible. In block E (Fig. 7), our graben data agrees very well with the graben and faults mapped by Dohm et al. (2001a). The influence of Tharsis may be evidenced as the minor peak in the NW direction, which is very close to the orientation of the southeastern-most graben of Claritas Fossae located just west of block E. The WNW peak in block E graben parallels Valles Marineris. This orientation may, however, be at least partly also due to older fracturing radial to Argyre basin. The NNE peak can be interpreted as a manifestation of a concentric fracture pattern surrounding Argyre, the most striking evidence of which is the Bosporos Rupes located mainly in this block. This concentric fracturing may perhaps also be seen in the roughly N–S peak in the graben data of block G. Another possible origin for the NNE peak in graben data of block E can be Argyre-induced conjugate shear fracturing (see below).

The channels display a dominantly NW direction throughout the whole study area. The channels often indicate a trend different from the main PIC rim orientations, and they may partly influence the structural data available from PICs by destroying the straight rim segments by various resurfacing processes. The channels are associated with the graben (as was also noted by Dohm and Tanaka 1999) especially in blocks A and B, and are also apparently controlled by the regional topographic trend induced by the Tharsis bulge. The Holden (and possibly also Ladon) basin(s) likely influenced the orientations of channels in at least blocks C and D (see Schultz and Glicken 1979). The NE

orientation in block G is clearly caused by channels directed from the "rim" to the floor of the Argyre basin.

Polygonal Craters' Structural Implications

The Argyre region has gone through a complex tectonic history. Thus, it is not surprising that the directional pattern revealed by the polygonal craters' straight rim segment orientations is not a straightforward one to interpret. Clear matches with other structural indicators are usually lacking or at least controversial. The graben orientations do not have a counterpart in the major peaks in the PIC data, but rather the graben are most numerous in orientations, where straight rim segments are scarce (Figs. 7–8). In blocks A, B and C where ridges are most numerous, there are approximately corresponding peaks in PIC rim strikes. However, this may be just coincidental. It seems that PICs, regardless of how old they are (Öhman et al. 2006), reflect an older structural pattern mostly different from the graben and the ridges. This is in unison with the conclusions of Dzurisin (1978) and Strom et al. (1990), according to whom the oldest tectonic structures pre-dating the end of heavy bombardment control the Mercurian polygonal crater rim orientations.

In areas surrounding Isidis and Hellas basins, PIC rim orientations clearly mark the radial fractures emanating from the basins (Öhman et al. 2005). Similarly, Argyre-radial components in the rose diagrams can also be seen, e.g., in blocks A and B (NW-oriented peaks A3 and B3 in Fig. 6). It appears that both the ancient Ladon basin (Schultz and Glicken 1979; Schultz et al. 1982; Schultz and Frey 1990) and probably also the Holden basin just north of our study area (Fig. 2) affect the PIC rim orientations as well. For example, both the strong NW peak (D3) in the rose diagram from block D, and the NNE peak (C1) from block C are radial to Ladon. It should be emphasized, that the peak C1 is radial to Argyre, Ladon, and Holden basins.

The approximately N–S orientated peaks in the central blocks F (peak F4) and G (peak G1) may well be caused by concentric fracturing surrounding the Argyre basin somewhat contradicting the "radial dominance" reported by Thomas and Masson (1984). However, considering that relatively large number of the PICs are located in the central northern part of these blocks (see Fig. 4), straight rim segments induced by fractures radial to the basin may also contribute to the N–S peaks.

The large peak-ring crater Galle is located in block G, on the eastern "rim" of the Argyre basin. The fracture network induced by the Galle impact undoubtedly has been superposed on the pre-existing structures. However, given the locations of the PICs in block G (see Fig. 4), that does not significantly complicate the interpretations: probable Galle-induced fracturing for most part coincides with the Argyre radial and concentric fracturing.

In Hellas basin area, fracturing radial to the basin clearly appeared to extend further than the concentric fracturing (Öhman et al. 2005). To better define radial and concentric components to the Argyre basin on its western side, we narrowed their possible azimuthal ranges by defining a smaller area (44°S–56°S, 54°W–68°W; see Fig. 4), covering parts of blocks E and F. The resulting rose diagram (using 10° class intervals) is presented in Fig. 9. The basin-radial component is the prominent E-W peak (EF2), but the supposed concentric orientation (~N-S) is presented by only a minor peak (EF4) in the diagram. Instead, the NE-SW (EF1) and especially the NW-SE (EF3) orientations are more evident.

The rose diagram from west of Argyre presented in Fig. 9 is actually astonishingly similar to the diagram from a 16° × 18° block centered at 39°S, 328°W having a similar location with respect to the Hellas basin (see Fig. 2 in Öhman et al. 2005), reproduced in Fig. 9. Both diagrams have four peaks: E-W, NW-SE, N-S, and NE-SW. Hence, a common origin for the fracture networks in both areas seems appealing. The E-W and smaller N-S peaks can be taken as evidence of radial and concentric fracturing, respectively. Radial fracturing is initially induced in the early stage of basin modification by the negative load in the basin's interior and the following up-doming and inward flow of the astenosphere (Melosh 1976, 1989). Concentric fractures, however, are formed later, when the basin is modified under basin-filling load (Melosh 1978; Freed et al. 2001).

The origin of NW-SE and NE-SW peaks in Fig. 9, however, is more speculative. We tentatively suggest that these are manifestations of conjugate shear fracturing (e.g., Price and Cosgrove 1990; Twiss and Moores 1992). Like the concentric fractures, the proposed conjugate shear fractures are the result of later modification by basin-filling load (Melosh 1978; Freed et al. 2001). However, observational evidence of shear fracturing (strike-slip faulting) surrounding impact basins has been almost totally absent (e.g., Freed et al. 2001).

Freed et al. (2001) provide an equation (their equation 2) for the approximation of the width of the area of conjugate shear fracturing around impact basins loaded by post-impact basin fill. This equation can be used as a rough first-order estimate of the reality of the suggested conjugate shear fractures. We can assume the Argyre basin to be filled by a flat body of volcanic material (beneath the presently observable glacifluvial/lacustric/eolian deposits) 250 km in radius. Using 150 km as the thickness of the elastic lithosphere (Neumann et al. 2004), the approximation of Freed et al. gives the width of about 275 km for the potential conjugate shear fracture zone surrounding the Argyre basin. It is unlikely that the stresses would be high enough in this entire zone for actual fracturing to take place, but on the other hand multi-phase post-impact modification of the basin would widen the zone of fracturing (Freed et al. 2001).

Our hypothesis of a reasonably wide zone of shear fracturing surrounding the Argyre basin (and the Hellas basin) is in an agreement with the conclusions of Thomas and Masson (1984). They proposed that the width of an

intensively fractured zone around Argyre is notably larger than around lunar or Mercurian basins, indicating that the Martian lithosphere was more easily fractured during and after the impact than the lunar or Mercurian lithospheres (Thomas and Masson 1984). Therefore, despite the large uncertainties involved, we tentatively suggest that the PIC rim orientation data (NW-SE and NE-SW peaks; Fig. 9) in Argyre and Hellas basin regions fit the location and geometry of basin-induced conjugate shear fractures. This possibility is emphasized by the fact that similar, otherwise relatively poorly explained peak orientations are present in the PIC rim orientation diagrams from blocks F (peaks F1 and F3; Fig. 7) and H (peaks H1 and H3; Fig. 8) as well.

If the hypothesis that conjugate shear fractures contribute to the PIC rim orientations in the southern part of the Argyre region holds true, then it follows that conjugate shear fractures induced by Argyre and Ladon basins should be present in the northern half of our present study area as well. However, they are not evident in the PIC data. This may simply be an effect of other orientations being more dominant in those areas. The absence of conjugate shear fractures induced by the ancient Ladon basin may also be merely an indication of a lack of basin load. This possibility is strengthened by the fact that Ladon produces a notably smaller Bouguer gravity anomaly than Argyre (Neumann et al. 2004).

The strong NW orientation west of Argyre (Fig. 9 peak EF3; also in block E as peak E3) is quite intriguing, as it is present in some form in all blocks except G. A NW orientation is one of the Thomas and Masson's (1984) three pre-Argyre tectonic orientations. However, that is the least important one. West (blocks E and F) and east (block H) of Argyre the NW orientation may well be another set of the proposed conjugate shear fractures. Its dominance in the combined "EF" block can be understood by additional influence of the tectonism that is also responsible for the Claritas Fossae graben. The absence of the NW component in block G may perhaps be the result of the Galle impact erasing older structural trends that do not coincide with Galle-induced structures.

Interestingly, the most significant of the pre-Argyre tectonic structures as defined by Thomas and Masson (1984), i.e., the NE component, does not stand out in the PIC data, although it may be contributing to such orientations. We also believe, in contrast to Thomas and Masson (1984), that the Argyre basin has had tectonic influence beyond their "outer scarp," and it can be seen in the rim orientations of PICs.

Another peculiar direction presented by the PIC rims is the N-S peak (A1) in block A. One possible explanation might be that it is related to the same tectonism, which has caused the prominent N-S trending graben in Coracis Fossae, located just west of block A. So the old (Dohm and Tanaka 1999; Dohm et al. 2001a) tectonic orientations indicated by the graben of Coracis Fossae are seen in PIC data, whereas the younger WNW-oriented and Tharsis-centered graben that are so distinct in our study area do not have a counterpart in the PIC rim orientations.

Table 2 summarizes the interpretation of the PIC data. Although an explanation for each of the major peaks seen in the diagrams is offered, this doesn't mean that the explanation is the only possible solution: influencing contributors to PIC trends may be diverse and complex. Especially the prominent E–W orientation in the northern half of the study area is an enigmatic one. One possibility is that it is related to the hypothesized Martian plate tectonics. The magnetic anomalies, which may be related to plate tectonism, have a general E–W orientation (Acuña et al. 1999; Connerney et al. 1999, 2005; Purucker et al. 2000; Fairén et al. 2002). In the Argyre region, however, the anomalies give only very faint indications of possible plate tectonics, and the derived possible directions of crustal weakness are oriented slightly more towards the southeast (see Connerney et al. 2005). Currently, however, the plate tectonic influence cannot be reliably ruled out, highlighted by the pre-Tharsis, terrestrial-like mountain ranges, Coprates rise and Thaumasia highlands, forming the eastern and southern margins of the Thaumasia plateau (Dohm et al. 2001a, 2001b). These mountain ranges record magnetic signatures and complex structure (Dohm et al. 2002, 2007; Baker et al. 2007).

Other contributors to the E–W structural signature could include the development of components of the Tharsis bulge, such as the Thaumasia plateau, (Dohm et al. 2001a, 2001b), as well as several distinct centers of tectonic activity like south-central Valles Marineris (Anderson et al. 2001). Yet another possibility, especially in the northernmost parts of the western blocks, is the radial fracture pattern originating from the hypothetical Solis Planum basin suggested by Frey et al. (2007). And it may of course be that although the E-W component seems consistent throughout the area, it has several origins. All in all, it seems reasonable to suggest that straight segments of impact crater rims tend to form in orientations where two or more directions of crustal weakness coincide forming a dominating structural pattern. Another implication is that PICs tend to reflect a generally old structural pattern.

The Formation Mechanisms of Polygonal Impact Craters

In our earlier study (Öhman et al. 2006), we ruled out degradation as a means to create polygonal craters. The current work emphasizes that processes like major regional tectonic deformation (Tharsis and Valles Marineris tectonism), which take place after the crater formation, do not significantly affect the crater shape with respect to polygonality, unless of course a fault actually cuts through a crater, for example. This is demonstrated by the difference between orientations indicated by the directional trends of the straight segments of polygonal crater rims, and graben

Table 2. Possible contributing factors to help explain dominating PIC rim strike orientations.

Block	Peak no.[1]	Orientation	Possible contibuting factors[2]
A	A1	000°–015°	Coracis Fossae
	A2	075°–120°	Medium pre-Argyre
	A3	135°–150°	Argyre radial, minor pre-Argyre
B	B1	(000°)–045°	Major pre-Argyre, Ladon radial
	B2	075°–090°	Argyre concentric, medium pre-Argyre
	B3	135°–150°	Argyre radial, Ladon concentric
C	C1	000°–030°	Argyre radial, Ladon radial, Holden radial
	C2	090°–105°	Argyre concentric, medium pre-Argyre
	C3	120°–150°	Ladon concentric
D	D1	(015°)–045°	Argyre radial, Ladon concentric, major pre-Argyre
	D2	090°–105°	Medium pre-Argyre
	D3	135°–165°	Ladon radial, Argyre concentric, minor pre-Argyre
E	E1	015°–045°	Argyre conjugate, major pre-Argyre
	E2	075°–105°	Argyre radial
	E3	135°–150°	Argyre conjugate, Claritas Fossae, minor pre-Argyre
F	F1	015°–030°	Argyre conjugate, major pre-Argyre
	F2	075°–105°	Argyre radial
	F3	120°–150°	Argyre conjugate, minor pre-Argyre
	F4	165°–180°	Argyre concentric
G	G1	000°–030°	Argyre concentric
	G2	090°–120°	Argyre radial
H	H1	015°–030°	Argyre conjugate, major pre-Argyre
	H2	075°–120°	Argyre radial
	H3	135°–150°	Argyre conjugate, minor pre-Argyre
	H4	165°–180°	Argyre concentric
"EF"	EF1	020°–040°	Argyre conjugate, major pre-Argyre
	EF2	080°–100°	Argyre radial
	EF3	130°–150°	Argyre conjugate, Claritas Fossae, minor pre-Argyre
	EF4	170°–180°	Argyre concentric

[1]Peak numbering refers to Figs. 7–9.
[2]Note that these should not be considered as the only solutions, as there are diverse and complex factors that contribute to PIC morphology.

and ridge orientations, the latter of which largely have younger formational ages than the crustal structures affecting the craters. Polygonality is a primary and permanent feature of some impact craters, as was also concluded by Eppler et al. (1983).

If both of the proposed mechanisms (Eppler et al. 1983) for polygonal crater formation were more or less universally true, then the rim strike patterns of simple and complex polygonal craters in the same area should be different. This is not the case (Fig. 10), and as such, requires explanation. Previously, we showed (Öhman et al. 2006) that illumination geometry does not play a major role at regional scale. Thus, a natural conclusion is that perhaps the PIC formational models require revision.

The model of enhanced excavation in the direction parallel to target fractures, which is suggested for the formation of simple polygonal craters (Eppler et al. 1983), is based on detailed field work only at the Meteor Crater (Shoemaker 1962, 1963; Roddy 1978). It is generally accepted that such a mechanism works there. Tentative support for this model comes also from the studies by Watters (2006), who observed major faults coinciding with the corners of the Endurance crater in Meridiani Planum on Mars. However, impact and explosion cratering experiments (Fulmer and Roberts 1963; Gault et al. 1968) indicate a more complex relationship between straight crater rims and target structures. Hence, it seems likely that there is an additional mechanism contributing at least to the formation of polygonal simple craters.

Impact crater rims are formed by a combination of three factors: the structural uplift of the target material, the injection of breccia dikes, and the ejecta (e.g., Melosh 1989). The structural uplift in practice often transpires as thrusting, although also folding is important. Thrusting has been a well-documented process in the formation of the simple Meteor and Tswaing craters, for example (Shoemaker 1962, 1963; Roddy 1978; Brandt and Reimold 1995). The importance of pre-existing joints, faults, foliation planes, and shear zones for the uplift of the rim of the simple New Quebec crater was noted by Currie and Dence (1963) and Dence (1964). In addition to simple craters, major thrusting has been observed on the rim of Bosumtwi, a well-preserved 11 km-diameter complex crater (Reimold et al. 1998). So, although larger complex craters go through significant gravity-driven collapse in the modification stage (e.g., Melosh 1989; Melosh and Ivanov 1999; Kenkmann et al. 2000; Osinski and Spray 2005), the

dominating structures observed on the simple and small complex crater rims are thrusts.

We propose that the shape of at least simple and relatively small complex polygonal craters can originate from thrusting along pre-existing target structures (Fig. 11, model 3). This would explain the observation that no statistically significant difference can be seen in the orientation data obtained from simple and complex PICs (Fig. 10). It also explains the observations of experimental craters in fractured targets, where straight crater rim segments are sometimes parallel, sometimes at an angle of about 45° (similar to what is reported at the Meteor Crater) with the target fractures (Fulmer and Roberts 1963). It is also possible that the thrusting and excavation models (models 1 and 3) could be active at the same time, leading to fairly complex crater shapes in simple targets, like the hexagonal crater in a target with two perpendicular fracture sets as was observed in the experiments by Gault et al. (1968). In general, however, the typical partial hexagon shape of PICs probably originates from thrusting or slumping along orientations with an angle of about 120° between the fractures. Fracture sets with an angle of about 120° are commonly formed in conjugate shear fracturing, as well as Riedel shearing (R and R' shears; e.g., Twiss and Moores 1992) associated with strike-slip faults.

There is also indirect remote sensing evidence favoring our new model. Figure 12 displays an example of very small, relatively crude PICs on the floor of Ius Chasma, northwest of our study area. The most apparent straight rim segments of the craters are parallel to the dominating orientation of the fractures. This implies that the Meteor Crater-type mechanism has not been the cause of the polygonal shape of the craters in this case.

To summarize, we believe that there are three different mechanisms involved in the formation of polygonal impact craters (Fig. 11). All of them require some pre-existing dominant orientations of structural weakness in the target material:

1. Enhanced excavation parallel to the strike of the fractures (model 1 by Eppler et al. [1983]). In a target with two perpendicular sets of fractures, this results in the straight crater rim segments making an angle of about 45° with the orientation of the fractures. While well-established at Meteor Crater, this does not seem to be the dominant process in the formation of simple Martian craters in the Argyre region. Applicable probably only to simple craters.
2. Collapse along the fracture planes, taking place in the modification stage (model 2 by Eppler et al.). Similar to our new proposed thrusting mechanism, this also results in straight rim segments being parallel to target fractures. Applicable to complex craters that have gone through substantial collapse.
3. Thrusting along the fracture planes. Similar to the first mechanism, this also takes place during the excavation stage. Contrary to the first mechanism, the enlargement of the crater occurs in a direction perpendicular to the strike of the fractures, resulting in straight crater rims being parallel to target fractures. Applicable to simple and small complex craters.

Interestingly, the observed "excess" of PICs (Fig. 6; see also Aittola et al. 2007) falls within the size range of our proposed new PIC formation mechanism. Thus, according to this study, there seems to be a connection between our new model 3 and the "bulge" in the PIC size distribution. However, more work is needed before further conclusions can be drawn.

The reasons why only some of the crater rims are straight while others follow the arc of a circle are probably related to target being fractured in a multitude of orientations (no dominating structural trends), fracture spacing, or some parts of the target being non-fractured or fractured in unfavorable orientations. These issues are further discussed by Fulmer and Roberts (1963; see also Watters 2006, and Öhman et al. 2005). Another important factor that should be kept in mind is that there can be notable differences in the tectonic evolution of the crater in different parts of the crater (Osinski and Spray 2005): some parts of the crater rim may be deformed mainly by anticlinal folding (thus likely leading to more circular rim segment), whereas in other parts faulting may be more important (Roddy 1977, 1979; see also Lana et al. 2006, 2007).

SUMMARY AND CONCLUSIONS

Several conclusions about the geology, tectonics, and the cratering process can be drawn based on a detailed study of the polygonal impact craters of the Argyre region, as well other tectonic indicators. The region records a complex geologic history. From a tectonic point of view, the most important contributing factors to the evolution of the area have been the fracture patterns created by the Argyre and Ladon impacts and the basins' subsequent evolution, the Tharsis-centered interaction of magmatism and tectonism, and to a lesser extent, the tectonism related to the formation of Valles Marineris. An older, pre-Argyre tectonic pattern whose origin is unknown also seems to have had an influence on the study region.

While ridges are generally present in the northern part of the study area, they are most abundant in the northwestern part. Their orientations are clearly controlled by the Tharsis-related (and Syria Planum) tectonism, i.e., they are concentric to Tharsis. Graben, too, are found mostly in the northern part, and they are similarly controlled by Tharsis, being radial to it. At the same time, they are almost parallel to the general trend of Valles Marineris, and so are probably influenced by basement structures that are linked to the formation of this vast canyon system, a major component of Tharsis (including magmatic-driven activity along the major crustal/lithospheric weakness at and surrounding its central part; Dohm et al. 2001b, 2007). Channels are either closely associated with

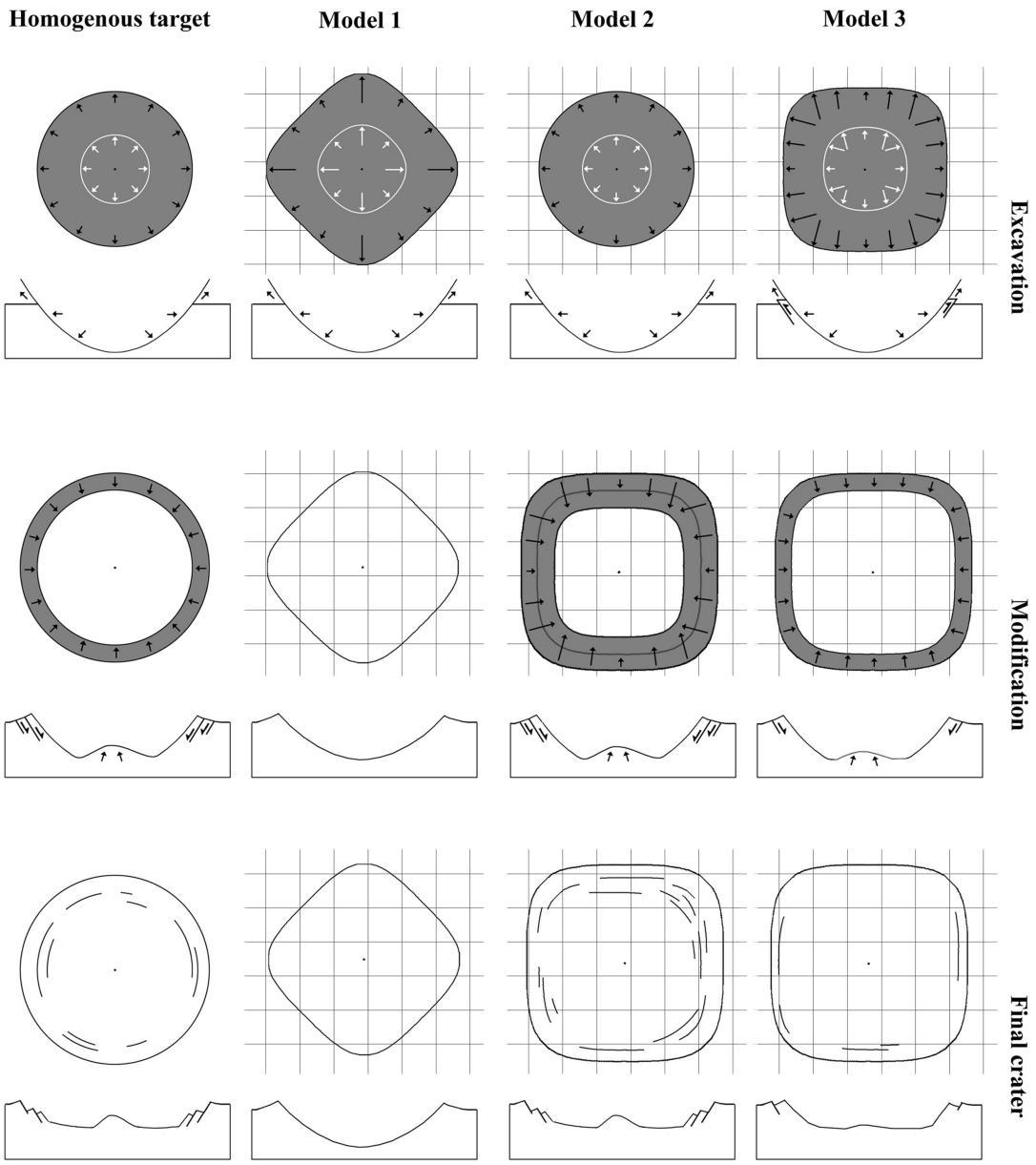

Fig. 11. A sketch of the plan views and profiles of the models for polygonal impact crater formation in an orthogonally fractured target (the background grid in models 1–3). The excavation stage of large complex craters (model 2) may be structurally controlled according either to model 1 or model 3, but the structurally controlled slumping in the modification stage overshadows this. Simple craters (models 1 and 3) and small complex craters (model 3) do not slump significantly, and thus the polygonal morphology obtained at the excavation stage prevails. The shading and the lengths of the arrows indicate the expansion of the crater. Models 1 and 2 are after Eppler et al. (1983).

graben (northwestern part), follow the general topographic slope induced by the Tharsis bulge, or indicate a flow to the floor of the Argyre basin.

Straight rim segment orientations of polygonal craters in the Argyre region reflect mostly basin-centered tectonism. The most prominent PIC rim orientations are radial to Argyre or Ladon basins. Concentric fracturing appears to be present as well, especially surrounding the Argyre basin. We tentatively propose that basin-induced conjugate shear fracturing can also be a possible candidate for explaining the observed direction patterns, and it may be even more important than concentric fracturing slightly further away from the basin. It appears that the most prominent clusters of PIC rim orientations emerge when two or more orientations of structural weakness coincide. Younger tectonism does not affect the polygonal crater shapes, emphasizing the idea that polygonality is a primary and permanent feature of craters (Eppler et al. 1983; Öhman et al. 2006).

The size distribution of polygonal craters (>7 km in diameter) in the Argyre region is not identical with that of the

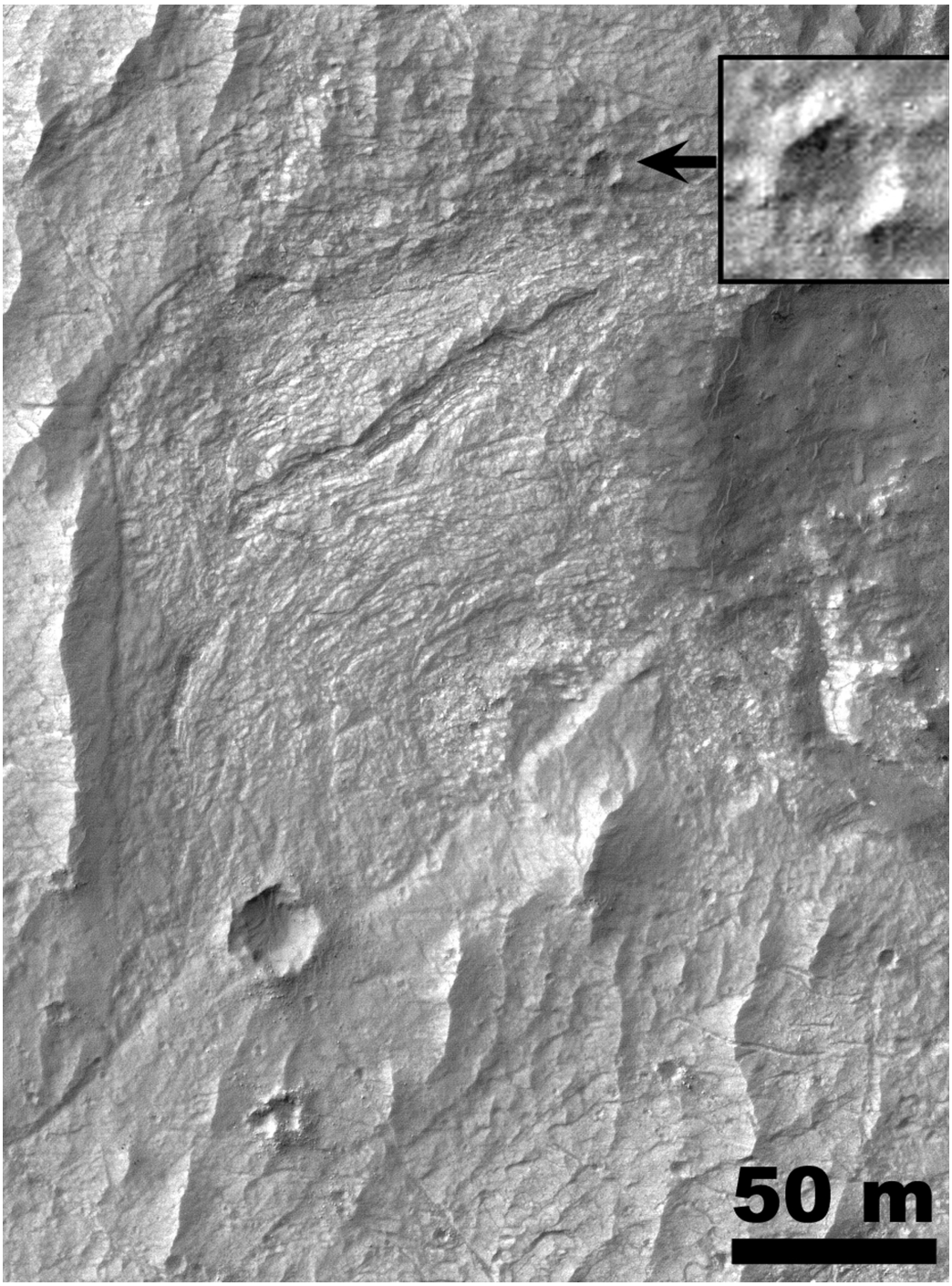

Fig. 12. Relatively small and rather poorly developed PICs on the floor of Ius Chasma (7.7°S, 80.5°W), which forms a part of the Valles Marineris canyon complex. Note that the most obvious straight segments of the crater rims are parallel to the dominating SW-NE-oriented fractures. Part of Mars Reconnaissance Orbiter's HiRISE image TRA_000823_1720. North is toward the top.

non-polygonal craters. There is an "excess" of PICs in approximately the diameter range of 15–35 km. This corresponds to 2–5 times the simple/complex transition diameter, which is the same size range as has been observed in a global study of Venusian PICs (Aittola et al. 2007), and is in agreement with lunar polygonal crater data (Pohn and Offield 1970; Öhman et al. 2007). Thus, in the cratering process there may be a "preferred" size range for the formation of polygonal craters, regardless of the target material or gravity. Further studies, however, are needed to prove or disprove this hypothesis.

On average in the Argyre region, polygonal craters larger

than 7 km in diameter make up about 17% of the entire crater population in that size range. There is some areal variation from ~13% up to ~22%, the largest percentages being in areas dominated by the oldest geologic units. Hence, polygonal craters seem to be more easily formed in areas that have had the longest time to be affected by tectonic processes. However, when the amount of polygonality is measured as a number of straight rim segments, no correlation between polygonality and geologic units appears. The different geologic units (at least the ones fairly closely related to each other) in the same area also seem to have the same PIC rim strike patterns.

Simple and complex PICs reveal similar patterns of their straight rim segments. This is in contrast with the predictions based on the current idea of simple polygonal crater formation (Eppler et al. 1983). Thus, we propose a new, additional PIC formation model, where PICs form in the excavation stage by thrusting along pre-existing planes of weakness. Thrusts are observed in both simple and complex crater rims, and therefore this model is applicable to both simple and small complex craters.

Acknowledgments–Dr. Joe Boyce raised some important questions regarding our work, and Dr. James Dohm contributed greatly, especially to the geotectonic context and the style of the manuscript. Their constructive reviews led to significant improvements of the manuscript and are thankfully acknowledged. Dr. Ann Bäckström is also thanked for useful comments, and Mr. Matias Hyvärinen for the preliminary selection and degradation classification of PICs used in this and our previous study. We also acknowledge the use of Viking imagery and Mars Global Surveyor's Mars Orbiter Laser Altimeter data obtained from NASA's Planetary Data System, the Mars Odyssey Thermal Emission Imaging System data processed at the Arizona State University, and the Mars Reconnaissance Orbiter's High Resolution Imaging Science Experiment data from the Lunar and Planetary Laboratory at the University of Arizona, as well as the efforts of the respective science teams. This research has also made use of data provided by NASA's Nordic Regional Planetary Image Facility in the University of Oulu, and NASA's Astrophysics Data System Bibliographic Services. The Vilho, Yrjö and Kalle Väisälä Foundation of the Finnish Academy of Science and Letters, the Finnish Graduate School in Geology, the Magnus Ehrnrooth Foundation and the Sohlberg Delegation of the Finnish Society of Sciences and Letters, the Space Institute of the University of Oulu, the Faculty of Science of the University of Oulu, the North Ostrobothnia Regional Fund of the Finnish Cultural Foundation, the Department of Physical Sciences of the University of Oulu, the Academy of Finland, and the Alfred Kordelin Foundation are thanked for partial financial support.

Editorial Handling—Dr. John Spray

REFERENCES

Abels A. 2003. Investigation of impact structures in Finland (Söderfjärden, Lumparn, Lappajärvi) by digital integration of multidisciplinary geodata. Ph.D. thesis, FB Geowissenschaften, Westfälische Wilhelms-Universität, Münster, Germany.

Acuña M. H., Connerney J. E. P., Ness N. F., Lin R. P., Mitchell D., Carlson C. W., McFadden J., Anderson K. A., Rème H., Mazelle C., Vignes D., Wasilewski P., and Cloutier P. 1999. Global distribution of crustal magnetization discovered by the Mars Global Surveyor MAG/ER experiment. *Science* 284:790–793.

Aittola M., Öhman T., Leitner J. J. and Raitala J. 2007. The characteristics of polygonal impact craters on Venus. *Earth, Moon, and Planets* 101:41–53, doi:10.1007/s11038-007-9148-4.

Anderson R. C., Dohm J. M., Golombek M. P., Haldemann A. F. C., Franklin B. J., Tanaka K. L., Lias J., and Peer B. 2001. Primary centers and secondary concentrations of tectonic activity through time in the western hemisphere of Mars. *Journal of Geophysical Research* 106:20,563–20,585.

Baldwin R. B. 1949. *The face of the Moon*. Chicago: The University of Chicago Press. 239 p.

Baldwin R. B. 1963. *The measure of the Moon*. Chicago: The University of Chicago Press. 488 p.

Baker V. R., Maruyama S., and Dohm J. M. 2007. Tharsis superplume and the geological evolution of early Mars. In: *Superplumes: Beyond plate tectonics,* edited by Yuen D. A, Maruyama S., Karato S.-I., and Windley B. F. Dordrecht: Springer. pp. 507–522.

Barlow N. G. 2003. Revision of the "Catalog of Large Martian Impact Craters" (abstract #3073). 6th International Conference on Mars. CD-ROM.

Basilevsky A. T. and Keller H. U. 2006. Comet nuclei: Morphology and implied processes of surface modification. *Planetary and Space Science* 54:808–829, doi:10.1016/j.pss.2006.05.001.

Belton M. J. S., Chapman C. R., Veverka J., Klaasen K. P., Harch A., Greeley R., Greenberg R., Head J. W., McEwen A., Morrison D., Thomas P. C., Davies M. E., Carr M. H., Neukum G., Fanale F. P., Davis D. R., Anger C., Gierasch P. J., Ingersoll A. P., and Pilcher C. B. 1994. First images of asteroid 243 Ida. *Science* 265: 1543–1547, doi:10.1126/science.265.5178.1543.

Binder A. B. and McCarthy D. W. Jr. 1972. Mars: The lineament systems. *Science* 176:279–281.

Brandt D. and Reimold W. U. 1995. The geology of the Pretoria Saltpan impact structure and the surrounding area. *South African Journal of Geology* 98:287–303.

Cheeney R. F. 1983. *Statistical methods in geology.* London: George Allen & Unwin. 169 p.

Chicarro A. F., Schultz P. H., and Masson P. 1985. Global and regional ridge patterns on Mars. *Icarus* 63:153–174.

Connerney J. E. P., Acuña M. H., Wasilewski P. J., Ness N. F., Rème H., Mazelle C., Vignes D., Lin R. P., Mitchell D. L., and Cloutier P. A. 1999. Magnetic lineations in the ancient crust of Mars. *Science* 284:794–798.

Connerney J. E. P., Acuña M. H., Ness N. F., Kletetschka G., Mitchell D. L., Lin R. P., and Reme H. 2005. Tectonic implications of Mars crustal magnetism. *Proceedings of the National Academy of Sciences*, doi:10.1073/pnas.0507469102.

Croft S. K. 1980. Cratering flow fields: Implications for the excavation and transient expansion stages of crater formation. Proceedings, 11th Lunar and Planetary Science Conference. pp. 2347–2378.

Croft S. K. 1985. The scaling of complex craters. *Journal of Geophysical Research* 90:C828–C842.

Currie K. L. and Dence M. R. 1963. Rock deformation in the rim of the New Quebec crater, Canada. *Nature* 198:80.

Davis J. C. 2002. *Statistics and data analysis in geology*, 3rd ed. New York: John Wiley & Sons. 638 p.

Dence M. R. 1964. A comparative structural and petrographic study of probable Canadian meteorite craters. *Meteoritics* 2:249–270.

Denk T., Neukum G., Helfenstein P., Thomas P. C., Turtle E. P., McEwen A. S., Roatsch T., Veverka J., Johnson T. V., Perry J. E., Owen W. M., Wagner R. J., Porco C. C., and the Cassini ISS Team. 2005. The first six months of Iapetus observations by the Cassini ISS camera (abstract #2262). 36th Lunar and Planetary Science Conference. CD-ROM.

Dohm J. M. and Tanaka K. L. 1999. Geology of the Thaumasia region, Mars: Plateau development, valley origins, and magmatic evolution. *Planetary and Space Science* 47:411–431.

Dohm J. M., Tanaka K. L., and Hare T. M. 2001a. Geologic, paleotectonic, and paleoerosional maps of the Thaumasia region, Mars. Geologic Investigations Series I-2650. Scale 1:5,000,000. U. S. Department of the Interior, U. S. Geological Survey.

Dohm J. M., Ferris J. C., Baker V. R., Anderson R. C., Hare T. M., Strom R. G., Barlow N. G., Tanaka K. L., Klemaszewski J. E., and Scott D. H. 2001b. Ancient drainage basin of the Tharsis region, Mars: Potential source for outflow channel systems and putative oceans or paleolakes. *Journal of Geophysical Research* 106: 32,943–32,958.

Dohm J. M., Maruyama S., Baker V. R., Anderson R. C., Ferris J. C., and Hare T. M. 2002. Plate tectonism on early Mars: Diverse geological and geophsical evidence (abstract #1639). 33rd Lunar and Planetary Science Conference. CD-ROM.

Dohm J. M., Kerry K., Keller J. M., Baker V. R., Maruyama S., Anderson R. C., Ferris J. C., and Hare T. M. 2005. Mars geological province designations for the interpretation of GRS data (abstract #1567). 36th Lunar and Planetary Science Conference. CD-ROM.

Dohm J. M., Baker V. R., Maruyama S., and Anderson R. C. 2007. Traits and evolution of the Tharsis superplume, Mars. In: *Superplumes: Beyond plate tectonics,* edited by Yuen D. A, Maruyama S., Karato S.-I., and Windley B. F. Dordrecht: Springer. pp. 523–536.

Dzurisin D. 1978. The tectonic and volcanic history of Mercury as inferred from studies of scarps, ridges, troughs, and other lineaments. *Journal of Geophysical Research* 83:4883–4906.

Elo S., Jokinen T., and Soininen H. 1992. Geophysical investigations of the Lake Lappajärvi impact structure, western Finland. *Tectonophysics* 216:99–109.

Elston W. E., Laughlin A. W., and Brower J. A. 1971. Lunar near-side tectonic patterns from Orbiter 4 photographs. *Journal of Geophysical Research* 76:5670–5674.

Eppler D. T., Ehrlich R., Nummedal D., and Schultz P. H. 1983. Sources of shape variation in lunar impact craters: Fourier shape analysis. *Geological Society of America Bulletin* 94:274–291.

Fairén A. G., Ruiz J., and Anguita F. 2002. An origin for the linear magnetic anomalies on Mars through accretion of terranes: Implications for dynamo timing. *Icarus* 160:220–223.

Fielder G. 1961. *Structure of the Moon's surface.* London: Pergamon Press. 246 p.

Fielder G. 1965. *Lunar geology.* London: Lutterworth Press. 184 p.

Floran R. J. and Dence M. R. 1976. Morphology of the Manicouagan ring-structure, Quebec, and some comparisons with lunar basins and craters. Proceedings, 7th Lunar Science Conference. pp. 2845–2865.

Freed A. M., Melosh H. J., and Solomon S. C. 2001. Tectonics of mascon loading: Resolution of the strike-slip faulting paradox. *Journal of Geophysical Research* 106:20,603–20,620.

Frey H., Edgar L., and Lillis R. 2007. Very large visible and buried impact basins on Mars: Implications for internal and crustal evolution and the late heavy bombardment in the inner solar system (abstract #3070). 7th International Conference on Mars. CD-ROM.

Fulmer C. V. and Roberts W. A. 1963. Rock induration and crater shape. *Icarus* 2:452–465.

Garvin J. B., Sakimoto S. E. H., and Frawley J. J. 2003. Craters on Mars: Global geometric properties from gridded MOLA topography (abstract #3277). 6th International Conference on Mars. CD-ROM.

Gault D. E., Quaide W. L., and Oberbeck V. R. 1968. Impact cratering mechanics and structures. In *Shock metamorphism of natural materials,* edited by French B. M. and Short N. M. Baltimore: Mono Book Corporation. pp. 87–99.

Grant J. A. and Parker T. J. 2002. Drainage evolution in the Margaritifer Sinus region, Mars. *Journal of Geophysical Research* 107:5066, doi:10.1029JE001678.

Grott M., Hauber E., Werner S. C., Kronberg P., and Neukum G. 2005. High heat flux on ancient Mars: Evidence from rift flank uplift at Coracis Fossae. *Geophysical Research Letters* 32: L21201, doi:10.1029/2005GL023894.

Gurov E. P., Koeberl C., and Yamnichenko A. 2007. El'gygytgyn impact crater, Russia: Structure, tectonics, and morphology. *Meteoritics & Planetary Science* 42:307–319.

Head J. W. and Pratt S. 2001. Extensive Hesperian-aged south polar ice sheet on Mars: Evidence for massive melting and retreat, and lateral flow and ponding of meltwater. *Journal of Geophysical Research* 106:12275–12299.

Hiesinger H. and Head J. W. 2002. Topography and morphology of the Argyre basin, Mars: Implications for its geologic and hydrologic history. *Planetary and Space Science* 50:939–981.

Hodges C. A. 1980. Geologic map of the Argyre quadrangle of Mars. Map #I-1181 (MC-26). Scale 1:5,000,000. Department of the Interior, U. S. Geological Survey.

Kargel J. S. 1993. Geomorphic processes in the Argyre-Dorsa Argentea region of Mars (abstract). 24th Lunar and Planetary Science Conference. pp. 753–754.

Kargel J. S. and Strom R. G. 1992. Ancient glaciation on Mars. *Geology* 20:3–7.

Kenkmann T., Ivanov B. A., and Stöffler D. 2000. Identification of ancient impact structures: Low-angle faults and related geological features of crater basements. In *Impacts and the early Earth,* edited by Gilmour I. and Koeberl C. Berlin Heidelberg: Springer Verlag. pp. 279–307.

Kirk R. L., Lee E. M., Sucharski R. M., Richie J., Grecu A., and Castro S. K. 2000. MDIM 2.0: A revised global digital image mosaic of Mars (abstract #2011). 31st Lunar and Planetary Science Conference. CD-ROM.

Kopal Z. 1966. *An introduction to the study of the Moon.* Dordrecht: D. Reidel Publishing Company. 466 p.

Lana C., Romano R., Reimold W. U., and Hippertt J. 2006. Collapse of large complex impact craters: Implications from the Araguainha impact structure, central Brazil. *Geology* 34:9–12, doi:10.1130/G21952.1.

Lana C., Souza Filho C. R., Marangoni Y. R., Yokoyama E., Trindale R. I. F., Tohver E., and Reimold W. U. 2007. Insights into the morphology, geometry, and post-impact erosion of the Araguainha peak-ring structure, central Brazil. *Geological Society of America Bulletin* 119:1135–1150, doi:10.1130/B26142.1.

Melosh H. J. 1976. On the origin of fractures radial to lunar basins. Proceedings, 7th Lunar Science Conference. pp. 2967–2982.

Melosh H. J. 1978. The tectonics of mascon loading. Proceedings, 9th Lunar and Planetary Science Conference. pp. 3513–3525.

Melosh H. J. 1989. *Impact cratering: A geologic process.* New York: Oxford University Press. 245 p.

Melosh H. J. and Dzurisin D. 1978. Mercurian global tectonics: A consequence of tidal despinning? *Icarus* 35:227–236.

Melosh H. J. and Ivanov B. 1999. Impact crater collapse. *Annual Review of Earth and Planetary Sciences* 27:385–415.

Mohit P. S. and Phillips R. J. 2007. Viscous relaxation on early Mars: A study of ancient impact basins. *Geophysical Research Letters* 34:L21204, doi:10.1029/2007GL031252.

Mouginis-Mark P. J. 1979. Martian fluidized crater morphology: Variations with crater size, latitude, altitude, and target material. *Journal of Geophysical Research* 84:8011–8022.

Neumann G. A., Zuber M. T., Wieczorek M. A., McGovern P. J., Lemoine F. G., and Smith D. E. 2004. Crustal structure of Mars from gravity and topography. *Journal of Geophysical Research* 109:E08002, doi:10.1029/2004JE002262.

Öhman T. 2007. The structural control of polygonal impact craters on Mars. Unpublished Licentiate thesis, Department of Geosciences, University of Oulu, Finland.

Öhman T., Aittola M., Kostama V.-P., and Raitala J. 2005. The preliminary analysis of polygonal impact craters within greater Hellas region, Mars. In *Impact tectonics*, edited by Koeberl C. and Henkel H. Berlin Heidelberg: Springer-Verlag. pp. 131–160.

Öhman T., Aittola M., Kostama V.-P., Hyvärinen M., and Raitala J. 2006. Polygonal impact craters in the Argyre region, Mars: Evidence for influence of target structure on the final crater morphology. *Meteoritics & Planetary Science* 41:1163–1173.

Öhman T., Aittola M., Kostama V.-P., Kallo M., and Raitala J. 2007. The mechanics of polygonal impact crater formation (abstract #8020). Bridging the Gap II: Effect of Target Properties on the Impact Cratering Process. LPI Contribution 1360. pp. 87–88.

Osinski G. R. and Spray J. G. 2005. Tectonics of complex crater formation as revealed by the Haughton impact structure, Devon Island, Canadian High Arctic. *Meteoritics & Planetary Science* 40:1813–1834.

Parker T. J., Clifford S. M., and Banerdt W. B. 2000. Argyre Planitia and the Mars global hydrologic cycle (abstract #2033). 31st Lunar and Planetary Science Conference. CD-ROM.

Pike R. 1980. Control of crater morphology by gravity and target type: Mars, Earth, Moon. Proceedings, 11th Lunar and Planetary Science Conference. pp. 2159–2189.

Pike R. J. and Spudis P. D. 1987. Basin-ring spacing on the Moon, Mercury, and Mars. *Earth, Moon, and Planets* 39:129–194.

Pohn H. A. and Offield T. W. 1970. Lunar crater morphology and relative-age determination of lunar geologic units—Part 1. Classification. *Geological Survey Research 1970.* U.S. Geological Survey Professional Paper 700-C. pp. C153–C162.

Porco C. C., Baker E., Barbara J., Beurle K., Brahic A., Burns J. A., Charnoz S., Cooper N., Dawson D. D., Del Genio A. D., Denk T., Dones L., Dyudina U., Evans M. W., Giese B., Grazier K., Helfenstein P., Ingersoll A. P., Jacobson R. A., Johnson T. V., McEwen A., Murray C. D., Neukum G., Owen W. M., Perry J., Roatsch T., Spitale J., Squyres S., Thomas P. C., Tiscareno M., Turtle E., Vasavada A. R., Veverka J., Wagner R., and West R. 2005. Cassini imaging science: Initial results on Phoebe and Iapetus. *Science* 307:1237–1242.

Price N. J. and Cosgrove J. W. 1990. *Analysis of geological structures.* New York: Cambridge University Press. 502 p.

Prockter L., Thomas P., Robinson M., Joseph J., Milne A., Bussey B., Veverka J., and Cheng A. 2002. Surface expressions of structural features on Eros. *Icarus* 155:75–93.

Purucker M., Ravat D., Frey H., Voorhies C., Sabaka T., and Acuña M. 2000. An altitude-normalized magnetic map of Mars and its interpretation. *Geophysical Research Letters* 27:2449–2452.

Reimold W. U., Brandt D., and Koeberl C. 1998. Detailed structural analysis of the rim of a large, complex impact crater: Bosumtwi crater, Ghana. *Geology* 26:543–546.

Roddy D. J. 1977. Pre-impact conditions and cratering processes at the Flynn Creek crater, Tennessee. In *Impact and explosion cratering,* edited by Roddy D. J., Pepin R. O., and Merrill R. B. New York: Pergamon Press. pp. 277–308.

Roddy D. J. 1978. Pre-impact geologic conditions, physical properties, energy calculations, meteorite and initial crater dimensions and orientations of joints, faults and walls at Meteor Crater, Arizona. Proceedings, 9th Lunar and Planetary Science Conference. pp. 3891–3930.

Roddy D. J. 1979. Structural deformation at the Flynn Creek impact crater, Tennessee: A preliminary report on deep drilling. Proceedings, 10th Lunar and Planetary Science Conference. pp. 2519–2534.

Roddy D. J. and Davis L. K. 1977. Shatter cones formed in large-scale experimental explosion craters. In *Impact and explosion cratering,* edited by Roddy D. J., Pepin R. O., and Merrill R. B. New York: Pergamon Press. pp. 715–750.

Schultz P. H. 1976. Moon morphology. Austin: University of Texas Press. 626 p.

Schultz P. H. and Glicken H. 1979. Impact crater and basin control of igneous processes on Mars. *Journal of Geophysical Research* 84: 8033–8047.

Schultz P. H., Schultz R. A., and Rogers J. 1982. The structure and evolution of ancient impact basins on Mars. *Journal of Geophysical Research* 87:9803–9820.

Schultz R. A. 1985. Assessment of global and regional tectonic models for faulting in the ancient terrains of Mars. *Journal of Geophysical Research* 90:7849–7860.

Schultz R. A. and Frey H. V. 1990. A new survey of multiring impact basins on Mars. *Journal of Geophysical Research* 95:14,175–14,189.

Scott D. H., Diaz J. M., and Watkins J. A. 1977. Lunar farside tectonics and volcanism. Proceedings, 9th Lunar and Planetary Science Conference. pp. 1119–1130.

Scott D. H. and Tanaka K. L. 1986. Geologic map of the western equatorial region of Mars. Scale 1:15,000,000. Map I-1802-A. Department of the Interior, U. S. Geological Survey.

Sheskin D. J. 2004. *Handbook of parametric and nonparametric statistical procedures,* 3rd ed. Boca Raton: Chapman & Hall/CRC. 1193 p.

Shoemaker E. M. 1962. Interpretation of lunar craters. In *Physics and astronomy of the Moon,* edited by Kopal Z. New York: Academic Press. pp. 283–359.

Shoemaker E. M. 1963. Impact mechanics at Meteor Crater, Arizona. In *The Moon, meteorites and comets,* edited by Middlehurst B. M. and Kuiper G. P. Chicago: The University of Chicago Press. pp. 301–336.

Spray J. G., Butler H. R., and Thompson L. M. 2004. Tectonic influences on the morphometry of the Sudbury impact structure: Implications for terrestrial cratering and modeling. *Meteoritics & Planetary Science* 39:287–301.

Spudis P. D. 1993. *The geology of multi-ring impact basins.* Cambridge: Cambridge University Press. 263 p.

Strom R. G., Malin M. C., and Leake M. A. 1990. Geologic map of the Bach (H-15) quadrangle of Mercury. Map I-2015. Scale 1: 5,000,000. Department of the Interior, U. S. Geological Survey.

Tanaka K. L. and Scott D. H. 1987. Geologic map of the polar regions of Mars. Map I-1802-C. Scale 1:15,000,000. Department of the Interior, U. S. Geological Survey.

Tanaka K. L., Scott D. H., and Greeley R. 1992. Global stratigraphy. In *Mars,* edited by Kieffer H. H., Jakosky B. M., Snyder C. M., and Matthews M. S. Tucson: The University of Arizona Press. pp. 345–382.

Thomas P. G. and Masson P. H. 1984. Geology and tectonics of the Argyre area on Mars: Comparisons with other basins in the solar system. *Earth, Moon, and Planets* 31:25–42.

Thomas P. C., Veverka J., Bell J. F. III, Clark B. E., Carcich B., Joseph J., Robinson M., McFadden L. A., Malin M. C., Chapman C. R., Merline W., and Murchie S. 1999. Mathilde: Size, shape, and geology. *Icarus* 140:17–27, doi:icar.1999.6121.

Twiss R. J. and Moores E. M. 1992. *Structural geology.* New York: W. H. Freeman and Company. 532 p.

Veverka J., Thomas P., Harch A., Clark B., Bell J. F. III, Carcich B., Joseph J., Chapman C., Merline W., Robinson M., Malin M., McFadden L. A., Murchie S., Hawkins S. E. III, Farquhar R., Izenberg N., and Cheng A. 1997. NEAR's flyby of 253 Mathilde: Images of a C asteroid. *Science* 278:2109–2114, doi:10.1126/science.278.5346.2109.

Watters W. A. 2006. Structure of polygonal impact craters at Meridiani Planum, Mars, and a model relating target structure to crater shape (abstract #2163). 37th Lunar and Planetary Science Conference. CD-ROM.

Watters W. and Zuber M. 2007. Relating polygonal crater morphology, tectonic setting and shallow crustal structure on Mars: A machine vision approach (abstract #EGU2007-A-04664). European Geosciences Union General Assembly, Vienna, Austria, 15–20 April 2007.

Werner S. C. 2008. The early Martian evolution—Constraints from basin formation ages. *Icarus* 195:45–60, doi:10.1016/j.*icarus*.2007.12.008.

Wichman R. W. and Schultz P. H. 1989. Sequence and mechanisms of deformation around the Hellas and Isidis impact basins on Mars. *Journal of Geophysical Research* 94:17333–17357.

Wilhelms D. E. 1973. Comparison of Martian and lunar multiringed circular basins. *Journal of Geophysical Research* 78:4084–4095.

Wilson C. W. Jr. and Stearns R. G. 1968. *Geology of the Wells Creek structure, Tennessee.* State of Tennessee, Department of Conservation, Division of Geology, Bulletin 68. Nashville: State of Tennessee, Department of Conservation. 236 p.

Wood C. A. and Head J. W. 1976. Comparison of impact basins on Mercury, Mars and the Moon. Proceedings, 7th Lunar Science Conference. pp. 3629–3651.

Zuber M. T., Smith D. E., Cheng A. F., Garvin J. B., Aharonson O., Cole T. D., Dunn P. J., Guo Y., Lemoine F. G., Neumann G. A., Rowlands D. D., and Torrence M. H. 2000. The shape of 433 Eros from the NEAR-Shoemaker Laser Rangefinder. *Science* 289: 2097–2101, doi:10.1126/science.289.5487.2097.